JOURNAL OF GEOPHYSICAL RESEARCH, VOL. 97, NO. C6, PAGES 9541-9563, JUNE 15, 1992

Low-Frequency Internal Oceanic Variability Under Seasonal Forcing

PAUL G. MYERS[1] AND ANDREW J. WEAVER[1]

Department of Atmospheric and Oceanic Sciences, McGill University, Montreal, Quebec, Canada

A series of numerical experiments are conducted using the Bryan-Cox ocean general circulation model to investigate the potential existence of low-frequency variability of the thermohaline circulation under seasonal forcing. Experiments are performed with different combinations of a seasonal cycle being present or not on the restoring temperature, the surface freshwater flux fields (mixed boundary conditions), and the surface wind forcing. Despite the presence of forcing on the dominant seasonal time scale, it is found that the system may oscillate at the decadal period or longer. The decadal variability is excited by changes in the net surface density flux which are due to the advection of temperature and salinity anomalies in the model domain. The magnitude of the seasonal cycle also plays an important role in determining the time scale of variability. Violent overturning events may occur on the century time scale under seasonal forcing. The magnitudes of the flushes are reduced compared with those found in similar experiments without the presence of a seasonal cycle.

1. INTRODUCTION

Over the last few years, interest in studying the effects of variability in the climate system has grown as it has been realized that Earth's climate has exhibited large changes in the past [e.g., *Crowley*, 1988] and will probably continue to change in the future. Variability exists in all five components of the climate system (atmosphere, hydrosphere, cryosphere, lithosphere, and biosphere), although on widely different time scales. These components are all coupled, with any variability in one component able to force changes that are global in scale in some or all of the other components.

There are two types of this variability with regard to the ocean: variations in external forcing (such as solar heating, winds, evaporation/precipitation, etc.) can cause oceanic variability. Then there is the internal variability of the oceanic system itself. The ocean plays a key role in climate due to its high heat capacity, which acts as a thermal buffer, and due to its role in the transfer of heat from low to high latitudes.

Numerous observations of low-frequency variability in the air-sea-ice climate system have been found in recent years. For example, variations on the decadal/interdecadal time scale have been observed in global surface air temperatures [*Ghil and Vautard*, 1991], west African rainfall and the landfall of intense hurricanes on the U.S. coast [*Gray*, 1990], Greenland ice core records [*Hibler and Johnsen*, 1979], Arctic sea ice extent [*Mysak and Manak*, 1989; *Mysak et al.*, 1990], runoff from the Eurasian land mass [*Cattle*, 1985; *Ikeda*, 1990] and global sea level pressure [*Krishnamurti et al.*, 1986]. Decadal/interdecadal variability has also been observed in the properties of North Atlantic Deep Water (NADW) formation [*Schlosser et al.*, 1991; *Lazier*, 1980; *Dickson et al.*, 1988], which have important implications for the thermohaline circulation and hence oceanic poleward heat transport.

Recently, ocean general circulation models (OGCMs) have been used to examine the stability and variability properties of the thermohaline circulation. These studies have evolved from the pioneering work of *Bryan* [1986] who showed how multiple equilibria of the thermohaline circulation could exist in the Bryan-Cox OGCM under mixed boundary conditions (a restoring boundary condition on temperature and a fixed flux on salinity).

In a few of the experiments of *Marotzke* [1990] and in the works of *Weaver and Sarachik* [1991*a*, *b*] and *Weaver et al.* [1991, 1992], spontaneous variability of the thermohaline circulation was found with a decadal time scale. This variability was shown to be characterized by the generation and advection of salinity and temperature anomalies which affected the deep water formation. More details of the mechanism involved in the generation and advection of these anomalies are given by *Weaver and Sarachik* [1991*b*].

Marotzke [1990] observed another phenomenon in his two-dimensional and three-dimensional models. In the absence of wind forcing, the thermohaline circulation could collapse, leading eventually to a period of intense convection during which the overturning increased to a strength of $O(150$ Sv). *Weaver and Sarachik* [1991*a*], who included wind forcing, and *Wright and Stocker* [1991], who did not, also observed a similar phenomenon and showed that when the circulation was in a collapsed state, low-latitude diffusion and the subsequent horizontal homogenization warmed the deep ocean past a certain critical point. This made the deep waters lighter than the overlying waters at high latitudes, thereby causing static instability, convection, and a rapid loss of much of the heat that the basin had built up in its collapsed state. The event was termed a flush.

In all of these studies, steady forcing was used. The radiant energy that drives the Earth's fluid envelopes comes from the Sun. This energy is not constant at any given latitude but varies on numerous time scales, with seasonal variations having important effects on the mean state of the atmosphere and ocean [*Gill*, 1982]. Changing from annual mean insolation to seasonal forcing has been demonstrated to change the mean state of a numerical model [*Wetherald and Manabe*, 1972]. So, is the presence of decadal/interdecadal variability in models that lack a seasonal cycle an artifact of these annually averaged boundary conditions or not? This paper will investigate this question. We show that decadal variability and flushes, internal to the system, can exist even in the presence of seasonal forcing.

[1]Now at School of Earth and Ocean Sciences, University of Victoria, Victoria, British Columbia, Canada.

Paper number 92JC00535.
0148-0227/92/92JC-00535$05.00

TABLE 1. Vertical Spacing Used in All Experiments

Model Level	Depth of Vertical Grid Box: Middle	Depth of Vertical Grid Box: Bottom	Δz
1	25	50	50
2	87.5	125	75
3	175	225	100
4	287.5	350	125
5	425	500	150
6	600	700	200
7	825	950	250
8	1100	1250	300
9	1450	1650	400
10	1875	2100	450
11	2325	2550	450
12	2775	3000	450
13	3250	3500	500
14	3750	4000	500
15	4250	4500	500

All depths are in meters.

The outline of this paper is as follows. In section 2 we briefly describe the numerical model, in section 3 we introduce and discuss the numerical experiments that were performed, and in section 4 we examine the effect different boundary conditions have on the poleward heat transport. We summarize our results in section 5.

2. Description of the Numerical Model

We use the *Cox* [1984] version of the Bryan-Cox ocean general circulation model to simulate a 4° latitudinal by 3.75° longitudinal horizontal resolution, 4500-m-deep, flat-bottomed ocean. The domain consists of a 60° wide (southern hemisphere) basin extending from the equator to 72°S. The vertical structure consists of 15 levels of increasing Δz (Table 1).

A symmetry condition is applied at the equator. No-slip and insulating conditions are used at the lateral walls. The bottom is assumed to be free-slip impermeable and insulating, while the rigid-lid approximation is used at the surface. We use a simple analytic formula for the zonal wind stress which is a function of latitude only [*Bryan*, 1987].

$$T^{\lambda}(\Phi) = 0.2 + 0.8 \sin(6\Phi) - \tfrac{1}{2}[1 + \tanh(10\Phi)] - \frac{1}{2}\left\{1 + \tanh\left[10\left(\frac{\pi}{2} + \Phi\right)\right]\right\} \text{ dyn/cm}^2$$

Here λ is the longitude and Φ is the latitude in radians. Despite its simplicity, this scheme captures the major features of the observed zonally averaged zonal wind stress (see Figure 15, profile E). For simplicity there is no meridional wind stress forcing. Annually averaged winds are used for reasons discussed later, except in experiment 9, where annually varying winds are used, and in experiment 10, where no wind forcing is present.

The vertical eddy diffusivity and viscosity are everywhere set to $A_{TV} = 1.0$ cm^2/s and $A_{MV} = 10.0$ cm^2/s, whereas the horizontal eddy viscosity and diffusivity are chosen to be $A_{MH} = 2.5 \times 10^9$ and $A_{TH} = 2 \times 10^7$ cm^2/s, respectively, over the whole domain. In all experiments, the *Cox* [1984] implicit convection parameterization scheme is used. When the density profile is determined to be statically unstable, the vertical diffusivity A_{TV} is set to 10^4 cm^2/s for one time step.

For all experiments the model was spun up from a resting homogeneous ocean with uniform temperature of 5°C and salinity of 34 ppt. The surface boundary condition on temperature is a Newtonian (restoring) condition with a relaxation constant of 25 days. That is, the temperature of the first model level is relaxed to a zonally uniform reference temperature, based on the *Haney* [1971] formulation. We vary this reference temperature in time with a period of a year to simulate the change in temperature over the course of a year.

At the southern boundary, the reference temperature was determined by a simple analytic cosine function designed to simulate a seasonal cycle (Figure 1*a*).

$$T_{\text{pol}} = [\cos(t\pi/182.5 + \pi) + 1](T_{\text{summary}}/2)$$

Here t is the day of the year, T_{pol} is the temperature at the polar boundary (0°C in the winter at $t = 0$), and T_{summer} (6.5°C) is the maximum temperature at the polar boundary in the summer. These values were composited from the *Levitus* [1982] atlas of world ocean data. A 365-day year is also assumed. As the observed magnitude of the seasonal variance in temperature at the equator is small (about 1°C [*Levitus*, 1982]), we assume a constant equatorial restoring temperature for simplicity. A cosine function of latitude was further fitted to the equatorial and polar temperatures to obtain interpolated temperatures at intermediate latitudes. The temperatures are illustrated in Figure 1*b* for spring ($t = 91$, end of March), summer ($t = 183$, end of June), fall ($t = 274$, end of September), and winter ($t = 365$, end of December).

An annually averaged restoring salinity surface boundary condition was used for the spin-up. The reference salinities were obtained by compositing annually averaged data from the *Levitus* [1982] atlas. No seasonal cycle was used on the restoring salinities during the spin-up so that we could focus on a minimum number of processes. We chose to use the seasonal cycle on temperature because much more is known about the thermal seasonal cycle than the freshwater flux seasonal cycle. Furthermore, we may still obtain a seasonal cycle on freshwater flux indirectly by diagnosing this over 1 year at our seasonal equilibrium.

To speed up convergence of the model, the acceleration technique (asynchronous integration) of *Bryan* [1984] was used. The barotropic vorticity and baroclinic velocity equations were integrated with a time step of 2 hours, while the tracer time step was either 2.5 or 1.25 days, throughout the water column. We discuss several synchronous integration results later.

The model was integrated for 6000 surface years until a steady seasonal cycle circulation had been reached. There were no trends in the salinity, temperature, or overturning stream function fields at the seasonal equilibrium. The model was then integrated for a further year during which the surface freshwater flux was diagnosed at each grid point of the basin and at each time step for each different tracer time step used. Slight differences existed between the freshwater fluxes diagnosed with different time steps due both to the dependence of convection on the time step [*Weaver and Sarachik*, 1991*a*] and to more intermediate points being used over the course of a year in the restoring temperature boundary condition under the smaller time step. These differences do not have a significant effect on the results.

So as not to have any net salt gain or loss into the basin over the course of 1 year, we compute this net annual salt flux and subtracted this small quantity from each grid box at

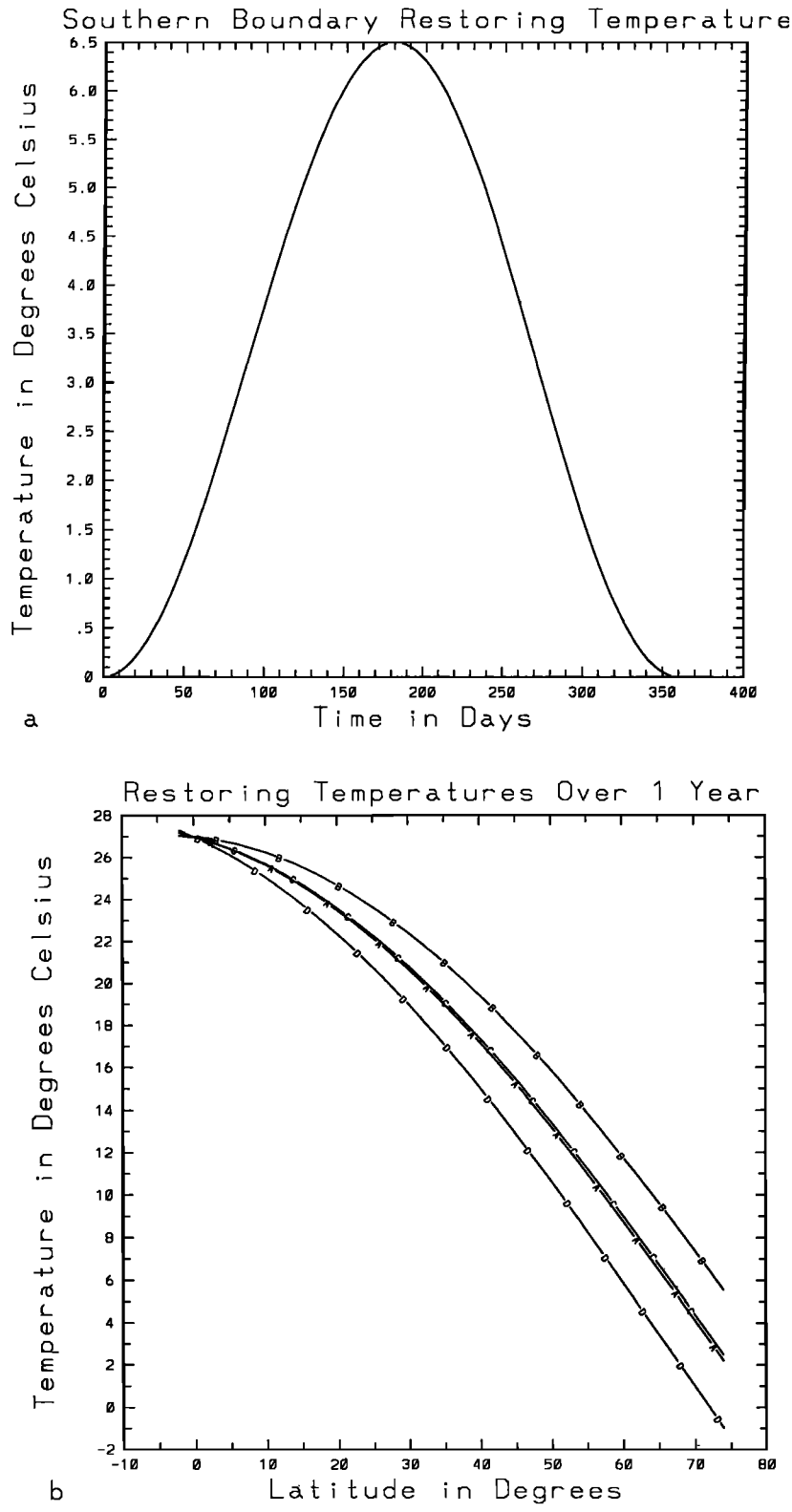

Fig. 1. (*a*) Restoring temperature (degrees Celsius) at the southern boundary over the course of a year. (*b*) Latitude dependence of the restoring temperatures of the basin over the course of a year: A, spring; B, summer; C, fall; D, winter.

each time step throughout the year. An instantaneously diagnosed freshwater flux is used instead of one obtained from an average over a further number of years of integration, as the differences between the two are insignificant [*Weaver et al.*, 1992]. The use of asynchronous integration during the diagnosis was also shown to have no effect on the results. All experiments were integrated for a further 6000 years under mixed boundary conditions.

TABLE 2. Characteristics of the 10 Experiments

Experiment	Seasonal Cycle*			Tracer Time Step, days	Integration†	Summer Temperature,‡ °C
	Temperature	FWF	Winds			
1	no	no	no	1.25	A	0.0
2	yes	yes	no	2.5	A	6.5
3	yes	no	no	1.25	A	6.5
4	yes	no	no	0.25	S	6.5
5	no	yes	no	1.25	A	0.0
6	no	no	no	1.25	A	3.25
7	yes	no	no	1.25	A	9.0
8	yes	no	no	1.25	A	4.0
9	yes	no	yes	0.25	S	6.5
10	yes	no	···	1.25	A	6.5

*Restoring boundary condition used on temperature, flux boundary condition used on freshwater flux, and boundary condition on surface wind stress ("yes" means seasonal; "no," not seasonal). Experiment 10 did not use wind forcing.

†A, asynchronous; S, synchronous.

‡Maximum summer restoring temperature at the polar boundary.

3. The Numerical Experiments

In this section the numerical experiments are described. A complete list of these experiments together with their distinguishing characteristics can be found in Table 2. All experiments exhibit internal low-frequency variability of one kind or another. We shall show that this variability is a high-latitude phenomenon linked inherently to the convection process. The magnitude and period of the variability depend on the nature of the surface boundary condition used and will be discussed in the following sections.

3.1. *Spin-up*

The basin was spun up for 6000 years until it had reached a seasonal equilibrium. The circulation is characterized by strong overturning. Although the net basin averaged surface heat flux varies greatly seasonally, there are no major seasonal variations in the overturning stream function between summer (Figure 2*a*) and winter (Figure 2*b*). The slight differences which are observed are due to the weakening of convection in the summer, leaving advection as the only process forming deep water. The process of decreased summer convection tended to reduce the zonal pressure gradients in the upper levels in summer, which subsequently reduced the meridional overturning slightly. Owing to the large inertia of the overturning, this seasonal convection was not able to significantly affect the mean advective deep water formation process, with net effect that the bottom water temperatures reflect mean "spring/fall" conditions (Table 3).

The seasonal changes in the surface heat flux are directly due to the changes in the restoring temperature, causing the ocean to lose much more heat to the colder "atmosphere" in the winter (62.7 W/m^2 basin averaged at equilibrium) and to gain heat from the "atmosphere" in the summer (42.5 W/m^2 basin averaged at equilibrium). Seasonal changes are seen in the upper levels of the zonal temperature fields, with the presence of a sharp seasonal thermocline in the summer (Figure 2*c*) changing in winter, at high latitudes, to the near vertical isotherms representative of convective activity (Figure 2*d*).

We calculated the net density flux into the basin for each season (Figures 3*a* to 3*d*) and for the annual average case (Figure 3*e*). These calculations are based on the formulae of *Schmitt et al.* [1989]. The density flux F_ρ is given by $F_\rho = -\rho(\alpha F_T - \beta F_S)$ where ρ is the density, and the thermal expansion and haline contraction coefficients are defined by

$$\alpha = -\frac{1}{\rho}\frac{\partial \rho}{\partial T}\bigg|_{P,S} \qquad \beta = \frac{1}{\rho}\frac{\partial \rho}{\partial S}\bigg|_{P,T}$$

Here $F_T = Q/\rho C_p$, where Q is the net heat flux into the ocean and C_p is the heat capacity of water. The flux of salt is due to the loss of fresh water from the sea surface and is given by $F_S = S(E - P)/(1 - S)$. $(E - P)$ is the freshwater flux in meters per second (E is evaporation and P is precipitation), and S is the salinity given in grams of salt per kilogram water. For these calculations the expansion coefficients, heat capacity and densities were evaluated using the surface temperature and salinity appropriate for the latitude, longitude, and time of year.

Our figures fortuitously agree quite well with those of *Schmitt et al.* [1989] in a qualitative sense. In the annual mean, they reveal a net density loss in the subtropical gyre, with density gains at higher latitudes and along the western boundary (Figure 3*e*). The density gain is greatest in the winter (Figure 3*d*) owing to the lower restoring temperatures. This is especially true in the high-latitude regions. During the spring (Figure 3*a*) and the summer (Figure 3*b*) there is a net density loss over almost the entire basin. In the fall (Figure 3*c*), with the onset of deep convection at high latitudes, there is a more intensified density gain there.

The individual contributions of heat and salt to the density flux are shown in Figure 3*f*, as the absolute value of the thermal/haline ratio ($|\alpha F_T/\beta F_S|$). This confirms that the restoring boundary condition equilibrium is thermally controlled. Again, our results agree well with those of *Schmitt et al.* [1989], with temperature dominating near the equator and in the high-latitude regions. The lack of a region of salinity domination in the subtropics is probably due to the poor parameterization of small-scale mixing processes in the model, which are believed to play a key role in the ocean [*Schmitt et al.*, 1989].

3.2. *Experiment 1 (Perpetual Winter)*

This experiment is a control run where no seasonal cycle is present on either temperature or the freshwater flux. A constant temperature of 0°C is used at the polar boundary. This temperature was chosen to allow for the development of a strong overturning circulation. An annual freshwater

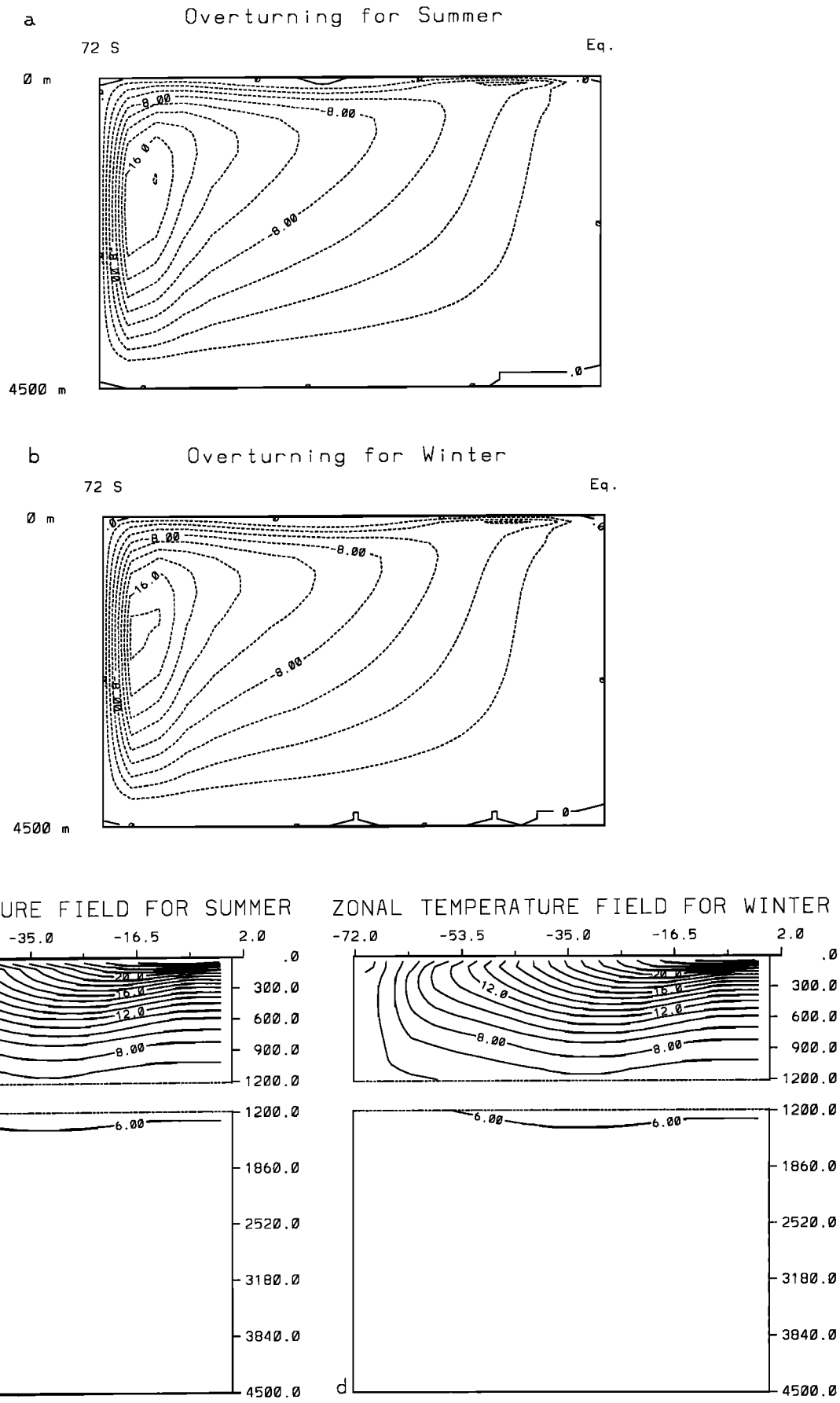

Fig. 2. Meridional overturning stream function during (*a*) summer and (*b*) winter, and zonal temperature profile during (*c*) summer and (*d*) winter at the end of spin-up. Contour intervals are 2.0 Sv for stream function and 1.0°C for temperature.

TABLE 3. Characteristic Time Scales of Variability in the 10 Experiments, With Basin Averaged Bottom Water Temperatures at the End of Experiments that Reached Seasonal Equilibrium

Experiment	Time Scale, years	Bottom Water Temperature, °C
Spin-up	none	5.1
1	29.4	2.6
2	20.8	5.1
3	11.4	8.1
4	11.4	8.1
5	330.0, 13.0	...*
6	1700.0	...
7	300.0, 11.4	...
8	500.0, 8.3	...
9	11.4	...
10	1800, 11.4	...

*No equilibrium.

flux is used (Figure 4). We term this our "perpetual winter" experiment.

Upon switching of the boundary conditions from restoring to mixed, the basin immediately flushed. This followed since after the removal of the seasonal cycle on temperature that was used during the spin-up, we now forced the surface waters with the 0°C temperature. This produced an unstable situation, with cool dense water overlying the warmer and lighter deep water produced during the spin-up. The circulation then settled down to an equilibrium with low-magnitude oscillations of less than 0.5 W/m^2. Strong decadal variability is not excited owing to the lack of a local maximum away from the southern boundary at high latitudes in the density flux field (not shown). Instead, the density flux field increased monotonically towards the southern boundary, with the maximum right at the southern wall.

3.3. *Experiment 2 (Fully Seasonal)*

In this, our "fully seasonal" experiment, we use the freshwater flux diagnosed from the spin-up every time step, and allow it to vary over the course of the year to simulate a seasonal cycle on the freshwater flux forcing. Figures 5*a* to 5*d* show the variations of the freshwater flux forcing field over the course of a year.

Characterizing the fields are low-latitude evaporation and high-latitude freshening. Intense precipitation occurs between 40°S and 70°S in winter (Figure 5*d*) but is counteracted by a weakening of the precipitation during the rest of the year. In fact, an evaporative region forms in the summer (Figure 5*b*). These occurrences are due to the presence of the restoring boundary condition on salinity during the spin-up. At high latitudes the restoring salinity falls between the predicted surface salinities for the summer and the winter. At the start of the summer the surface waters are relatively fresh owing to the absence of convection, with a salinity less than the restoring value. This leads to the model diagnosing the band of evaporation seen in Figure 5*b*. During the winter the processes of convection and advection act to produce a pool of water with surface salinity greater than the restoring value, which leads to the model diagnosing the precipitation seen in winter (Figure 5*d*). Fortuitously, our diagnosed freshwater fluxes agree quite well qualitatively with the observations of *Schmitt et al.* [1989].

The seasonal steady state obtained under restoring boundary conditions remained relatively stable upon the switch to mixed boundary conditions. To investigate the effects of the asynchronous integration techniques of *Bryan* [1984], a further integration was conducted synchronously from the end of the mixed boundary condition experiment, with a time step of 6 hours on all equations for 1000 years. A new *P-E* field was diagnosed for this run. The circulation remained stable upon the switch in time step.

Further investigation revealed, however, that the system was not completely stable under mixed boundary conditions, for weak oscillations were superimposed on the seasonal equilibrium basic state. Changes in the overturning stream function were small (<0.1 Sv) but the net basin averaged surface heat flux oscillated by ±2 W/m^2 over a 20.83-year period (Figure 6*a*). The synchronous integration confirmed this time scale but revealed a much smaller magnitude of variability, about 0.25 W/m^2 (Figure 6*b*).

It is not clear whether the very small differences between the synchronous and asynchronous integrations are due to the change in integration procedure or are simply due to the time step dependence of convection [*Weaver and Sarachik*, 1991*a*]. Also, we use a finer interpolation on both the seasonal restoring temperature and the seasonal freshwater flux in the synchronous integration experiment, perhaps yielding the small changes in the oceanic response. Nevertheless, since these fluctuations are so small, we conclude that the restoring boundary condition seasonal equilibrium is stable upon the switch to seasonally varying mixed boundary conditions.

3.4. *Experiment 3 (Seasonal Temperature)*

In the next series of experiments, a seasonal cycle is placed on one, but not both of the surface boundary conditions. To obtain a constant annual mean, we average the seasonal freshwater fluxes over the course of the year (Figure 4). In experiment 3, our "seasonal temperature" experiment, the basin was integrated with a seasonal cycle on temperature only, with a tracer time step of 1.25 days.

Upon the change from restoring to mixed boundary conditions, the circulation collapsed. Following this, the circulation increased in strength and began to oscillate irregularly. After several thousand years, the circulation steadied, entering a long period of fairly regular oscillations. The net basin-averaged surface heat flux taken every year at the height of the respective seasons revealed variability of 2 W/m^2 in the summer (Figure 7*a*) and 20 W/m^2 in the winter (Figure 7*b*), as compared with the 105.2-W/m^2 variance in surface heat flux over the course of the annual cycle.

The corresponding power spectral densities of these time series are given in Figures 7*c* and 7*d*. They show very strong decadal peaks at around 11 years, especially in the winter-plus weaker interannual peaks. Although it is not strictly correct to discuss time scales when using asynchronous integration, the results from the synchronous integration conducted in experiment 4 will show that these time scales are valid.

The oscillations are characterized by changes in the meridional overturning stream function. Over a single cycle, deep water formation occurs and then suddenly shuts off, followed by the development of a reverse cell that increases with time (as in the work of *Weaver and Sarachik* [1991*b*]).

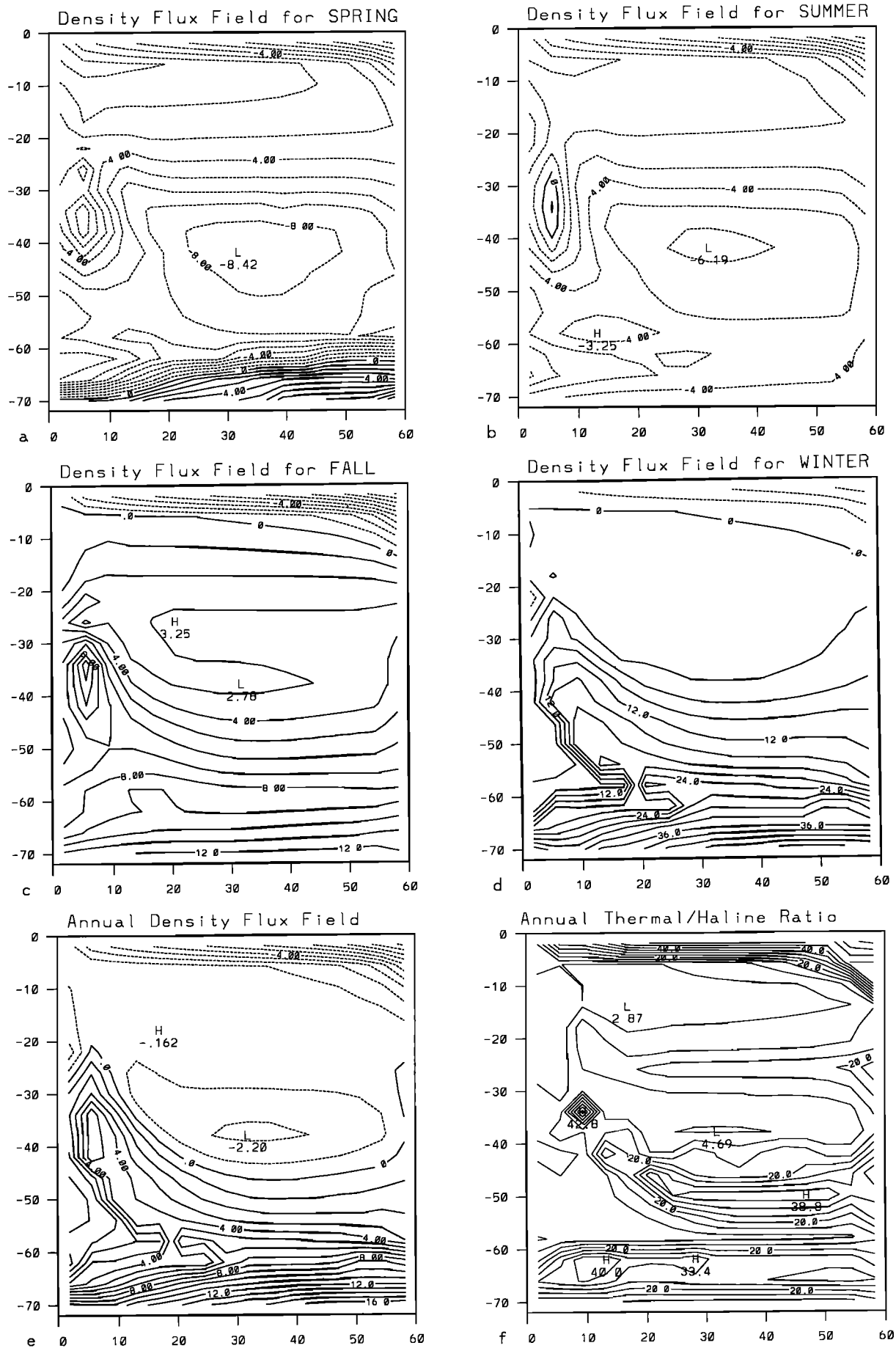

Fig. 3. Density flux field (10^{-6} kg/m^2 s) at the end of spin-up during (*a*) spring, (*b*) summer, (*c*) fall, (*d*) winter, and (*e*) the annual average, and (*f*) the absolute value of the ratio of the thermal and haline fluxes. The density flux contour interval is 1.0×10^{-6} kg/m^2 s, except in Figure 3*d*, where it is 3.0×10^{-6} kg/m^2 s; the contour interval in Figure 3*f* is 5.0.

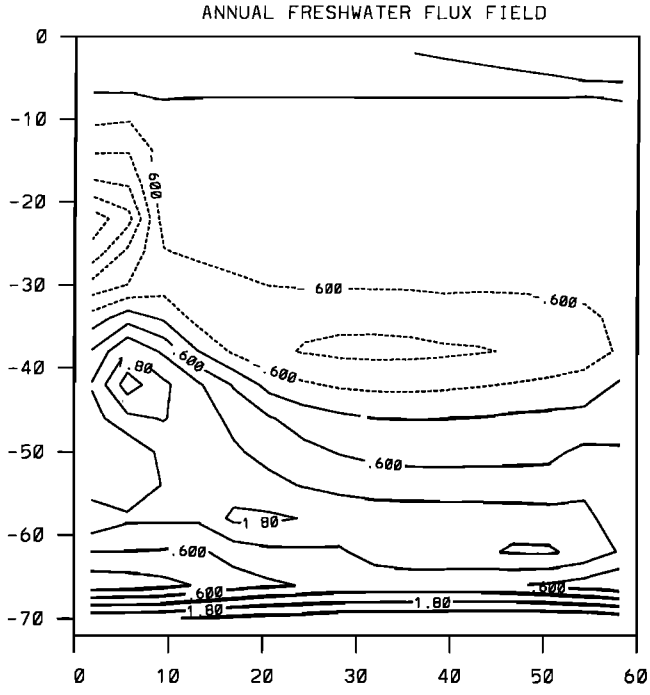

Fig. 4. Temporally averaged annual mean surface freshwater fluxes (meters per year) as diagnosed from the spin-up.

The whole process then repeats itself. The time needed for the full cycle is about 11 years. Figure 8 shows the development of the overturning stream function over an oscillation. Over the course of an oscillation the thermohaline circulation slowly decreases in strength by a factor of 2. Although weakened, the thermohaline circulation never actually collapses during the oscillation. As the thermohaline circulation weakens, a reverse cell begins to form at the polar boundary, rapidly growing in strength until it is nearly equal in magnitude to the main cell (Figure 8*b*). The reverse cell quickly fades away (Figure 8*c*), leaving a strengthening main cell which continues to grow until the oscillation begins anew.

This variability is linked to the existence of a local minimum in the *P-E* forcing field (Figure 4) and to cooling between 60° and 70°N. Starting when the overturning is decreasing from its maximum strength (Figures 8*c* and 8*d*), a warm, salty anomaly begins to form in the evaporative region near 45°S and east of 20° (Figure 4), due to a process similar to the *Welander* [1982] oscillator. This anomaly then begins to move eastward and slowly poleward. It is cooled and freshened as it moves. Only when it reaches the high-latitude *P-E* minimum is the freshening not strong enough to overcome the cooling produced by the low restoring temperatures at these latitudes. This allows the thermal effects to dominate over the haline effects (Figure 9*a*), producing a positive maximum in the density flux (Figure 9*b*). This positive density flux in turn drives deep convection and subsequent overturning.

The high precipitation found poleward of the evaporative region (Figure 4) prevents the anomaly from expanding meridionally, and hence it grows zonally. As this region of density gain grows and more deep convection occurs, the zonal pressure gradients weaken, decreasing the strength of the thermohaline circulation. Eventually, the anomaly is cut off from its source and hence begins to decay, increasing the zonal pressure gradients and hence the meridional overturning. The presence of the minimum in the *P-E* fields prevents the total dissolution of the anomaly and hence a breakdown of the thermohaline circulation. A more complete description of the oscillation is given by *Myers* [1992] and *Weaver and Sarachik* [1991*b*].

3.5. *Experiment 4 (Synchronous Seasonal Temperature)*

In experiment 4, our "synchronous seasonal temperature" experiment, we repeated experiment 3 but all equations were now integrated synchronously with a time step of 6 hours. This experiment reveals that the results from the asynchronous runs are robust. Only slight differences exist between the two runs, none of which have any significant effect on the overturning stream function. The surface heat flux (Figure 10*a*) agrees very well with that from the previous run (Figure 7*b*). The power spectral density of this series (not shown) revealed that the same periods of oscillation were dominant. As well, plots of the differences in zonal temperature between experiment 3 and experiment 4 for the summer (Figure 10*b*) and winter (Figure 10*c*) of a 1-year additional integration show almost no difference. The slight difference near 62°S is in the region of most marked variability during an oscillation. Given the chaotic nature of the oscillation, it is not surprising that we see small differences there.

The successful application of a seasonal cycle with asynchronous integration is due to our use of constant annual winds. Communication with K. Dixon at the NOAA Geophysical Fluid Dynamics Laboratory reveals that time step splitting works best when the winds change slowly or not at all. This is because winds, and especially variations in them, cause deviations from the basic asynchronous assumption that the velocity field is largely determined from the density field. This is especially true in coupled atmosphere-ocean models [*Bryan et al.*, 1975; *Washington and Meehl*, 1989], which are much more sensitive to the time step splitting owing to the coupling between the two components of the model. Atmospheric disturbances can cause the surface wind stress boundary condition for the OGCM to change rapidly. By keeping the winds constant, we reduce the variations in the surface momentum fluxes that the surface waters are forced to respond to (K. Dixon, personal communication, 1991).

3.6. *Experiment 5 (Seasonal Freshwater Flux)*

In experiment 3 we tested the effect of having a seasonal cycle on temperature. Now we look at the effect of having a seasonal cycle only on the freshwater flux. This is done by keeping the polar boundary restoring temperature constant at 0°C over the entire year. A 1.25-day tracer time step was used. We term this our "seasonal freshwater flux" experiment.

The resulting behavior of the model was quite different from that seen in the previous experiments. The circulation collapsed upon switching from restoring to mixed boundary conditions and entered a sequence of flushes and collapses, with fairly regular period. The net basin-averaged surface heat flux for this run can be seen in Figure 11*a*. Superimposed on this flush/collapse pattern are irregular oscillations of a fairly large magnitude. The power spectral density of this series (Figure 11*b*) reveals that the system is characterized by low-frequency oscillations on the century time scale and longer, while the smaller oscillations fall in the decadal/interdecadal range.

At first, this result seems contradictory to experiment 2 (fully

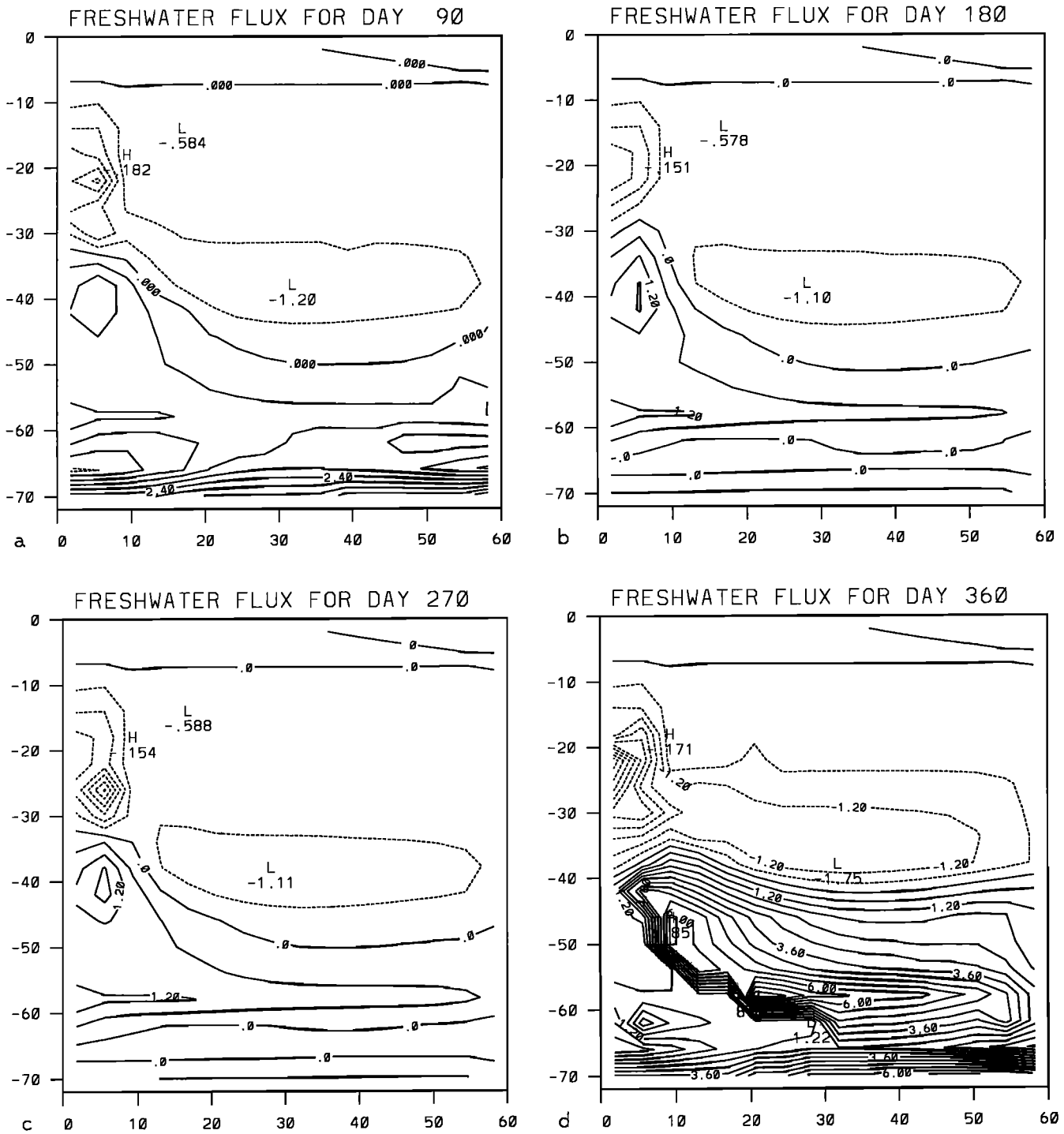

Fig. 5. Surface freshwater fluxes (meters per year) as diagnosed from the spin-up for different times of the year: (*a*) spring, (*b*) summer, (*c*) fall, and (*d*) winter.

seasonal) with its steady circulation. Both experiments have essentially the same cycle on the salinity flux. In experiment 5 the polar boundary is kept at 0°C year round, which would seem to provide better conditions for convection and hence for a more vigorous circulation. However, near the freezing point, the density of surface water depends less upon temperature than salinity, so with the seasonal cycle on freshwater flux, convection occurs preferentially in the season when the surface freshening is the least, i.e., in the summer (Figure 5*b*). With only weak convection in the winter, when freshening is strongest (Figure 5*d*), a large pool of fresh water is allowed to form. Since the seasonal time scale lies between the characteristic time scales for the adjustment of the baroclinic velocity field and for density changes due to advection [*Hasselmann*, 1982], the density anomaly produced by the freshening will not have been advected away by the next summer, leaving a freshwater cap which will curtail convection. This process continues as a positive feedback until the circulation collapses.

In experiment 2, where there was a seasonal cycle on temperature as well, deep convection tended to occur at the coldest period of the seasonal cycle, i.e., during the winter. Hence the fresh water produced in that season was con-

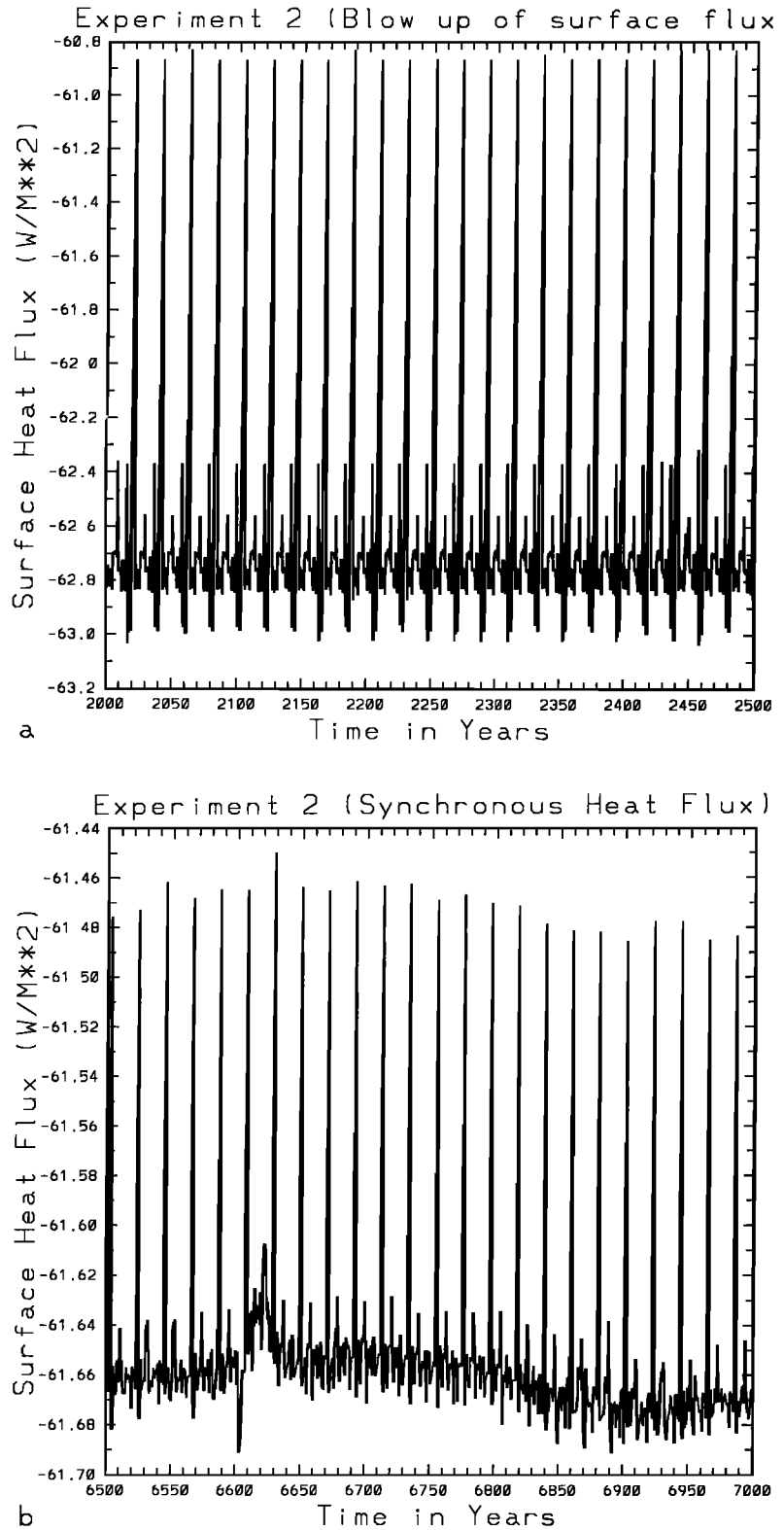

Fig. 6. Net basin-averaged surface heat flux (watts per square meter) for experiment 2 (fully seasonal): (*a*) 500 years of asynchronous integration and (*b*) 500 years of synchronous integration. Note that both time periods are subsets of the full integration period.

vected away, preventing the formation of a freshwater cap and the excitation of the positive feedback loop. This convection was aided by the high-salinity pool that was produced in the summer and not completely advected away by the winter. These mechanisms allow the maintenance of the strong, vigorous circulation that we observed in experiment 2.

To support these ideas, an analysis of convection statistics

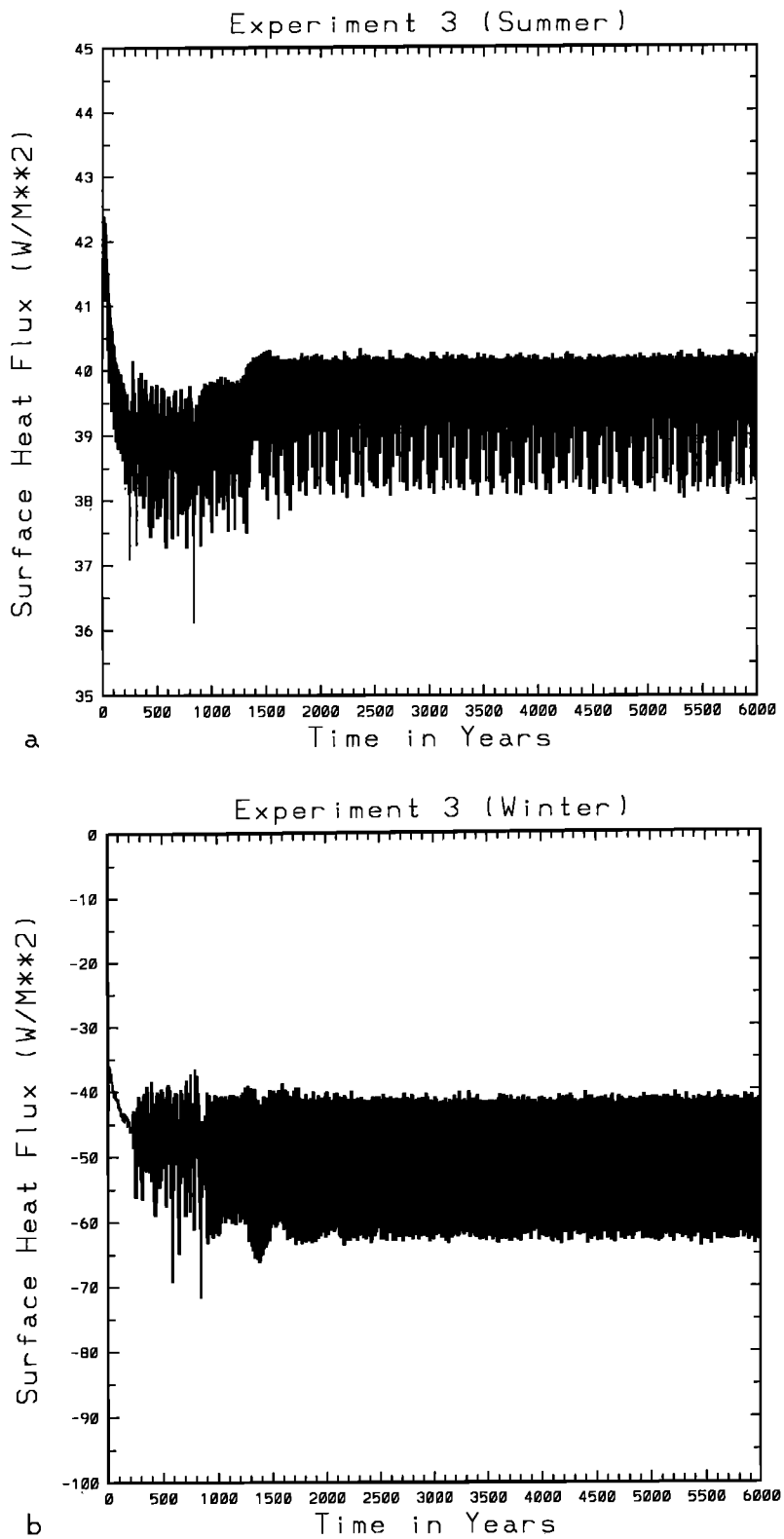

Fig. 7. Net basin-averaged surface heat flux (watts per square meter) during experiment 3 (seasonal temperature) for (*a*) every summer and (*b*) every winter for the 6000 years of integration, and power spectral density (using a 512-point fft) of the time series portrayed in (*c*) Figure 7*a* and (*d*) Figure 7*b*. The *x* axis in Figures 7*c* and 7*d* corresponds to the number of cycles over the 6000 years of integration.

was carried out. This was accomplished by determining the grid cells, in both experiments, during both the summer and winter, in which convection occurred. In experiment 2 (fully seasonal) we found that convection occurred exclusively in winter. Convection was found to occur in both the winter and the summer in experiment 5 but was very weak and sporadic in winter and so unable to prevent the formation of the freshwater cap that we had hypothesized.

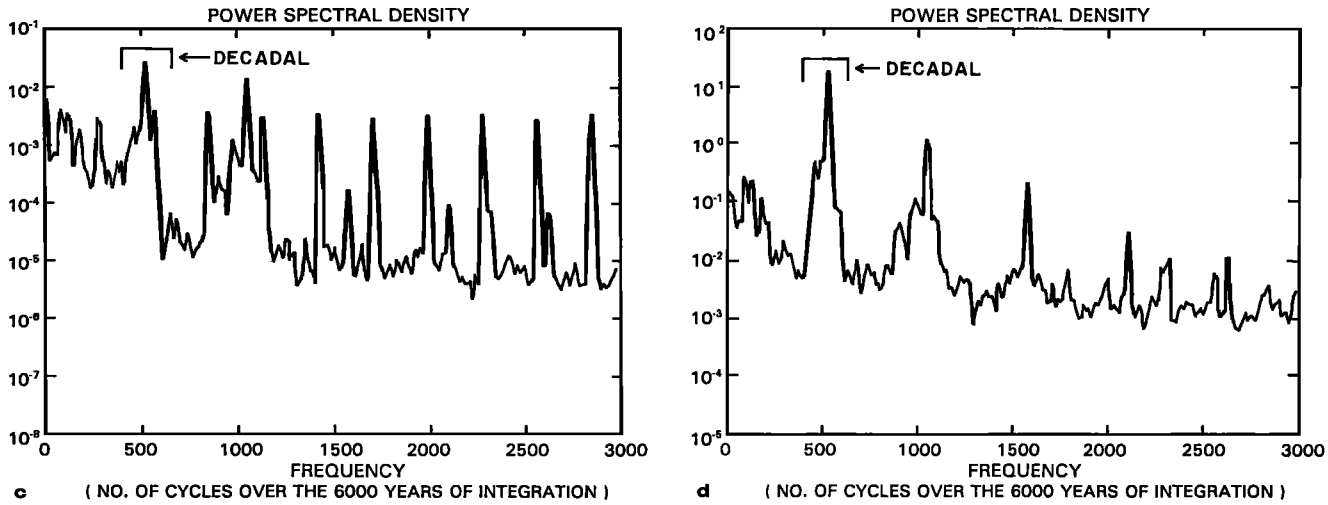

Fig. 7. (continued)

3.7. *Experiment 6 (Perpetual Spring)*

This experiment is similar to the perpetual winter experiment (experiment 1) except that a different polar boundary restoring temperature is used. Here, instead of the winter temperature, we use the average temperature over the seasonal cycle used in the other experiments, i.e., 3.25°C, with the freshwater flux field from experiment 3 (Figure 4). We term this our "perpetual spring" experiment. As compared with experiment 1, we have a weaker meridional thermal gradient, so we would expect high-latitude freshening to dominate here, which is the case.

The circulation collapsed almost immediately. The basin remained in the collapsed state for a long time before a flush occurred. The system then returned to the collapsed state, slowly building up to another flush (Figure 12*a*). The magnitude of the flushes were larger than those of experiment 5 (Figure 12*b*), and in fact were the largest of all experiments by almost a factor of 2. Weak, irregular oscillations were superimposed on the basic structure.

The frequency of the flushes is based on a diffusive time scale, with the ocean continually gaining heat in its collapsed state. This leads to a warm, salty deep ocean, which eventually becomes statically unstable, leading to ever growing convective activity at high latitudes. The excess heat gained by the basin in the collapsed state is rapidly given off to the "atmosphere."

Of interest to note is that the flushes that occurred in experiment 5 (seasonal freshwater flux), besides being significantly weaker, occurred at a much higher frequency than those in this experiment. Since diffusion appears to be the dominant time scale, why should the flushes occur at such different frequencies? An examination of the deep water temperatures reveals that the flushes occurred when the bottom waters reached 9°C in experiment 6 but at only 6°C in experiment 5. The reason is the presence of the seasonal cycle on the freshwater flux that exists in experiment 5. In the constant flux case, there is high-latitude freshening year round, which, together with the high polar restoring temperatures, leads to a very stable situation. In the seasonally varying case, high-latitude evaporation occurs in the late summer. This can be sufficient to cause static instability, convection, and a subsequent flush. The magnitude of the flush is weaker as the deep ocean temperature is cooler, so the ocean loses less heat in the weaker flushing event. This process is similar to the strong stochastic forcing case of *Weaver et al.* [1992].

3.8. *Experiment 7 (Amplified Seasonal Temperature)*

The purpose of this experiment and the following one are to investigate the effect the magnitude of the seasonal cycle has on the results. In this, our "amplified seasonal temperature" experiment, the amplitude of the cycle on temperature is increased by raising the summer temperature at the polar boundary, as is suggested, for example, to occur in the proposed greenhouse scenarios, to 9.0°C. In all other aspects, this experiment is the same as experiment 3 (fully seasonal).

The results are however, quite different from those of experiment 3 and in fact resemble those of experiment 5 (seasonal freshwater flux) most closely. Upon the switch in boundary conditions from restoring to mixed, the circulation collapsed and remained quiescent for a period of time. The magnitude of the stream function then began to oscillate. After about 2000 years, the circulation went through a series of collapses and flushes, with the flushes about 350 years apart (Figure 13*a*). Smaller-scale oscillations in the decadal range (Figure 13*b*) are superimposed on the flushes and collapses.

At low temperatures, salinity dominates in the nonlinear equation of state which we use [*Bryan and Cox*, 1972], but at higher temperatures small changes in temperature cause large changes in density. In both experiments 3 and 7 we are always freshening at high latitudes, but in experiment 7 it is also warmer at these high latitudes. This produces a very stable density profile at high latitudes that cannot be compensated for by cooling in winter. This prevents strong overturning and causes the development of a polar halocline catastrophe, similar to that of *Bryan* [1986]. However, over the long term, this situation is not stable with the diffusion of heat into the deep ocean, leading eventually to a flush, and the cycle then repeating itself. In experiment 3 the lower summer temperatures do not decrease the density enough to prevent winter cooling and wind-driven salt transport from producing convection. The circulation is then allowed to reestablish itself before a flush occurs.

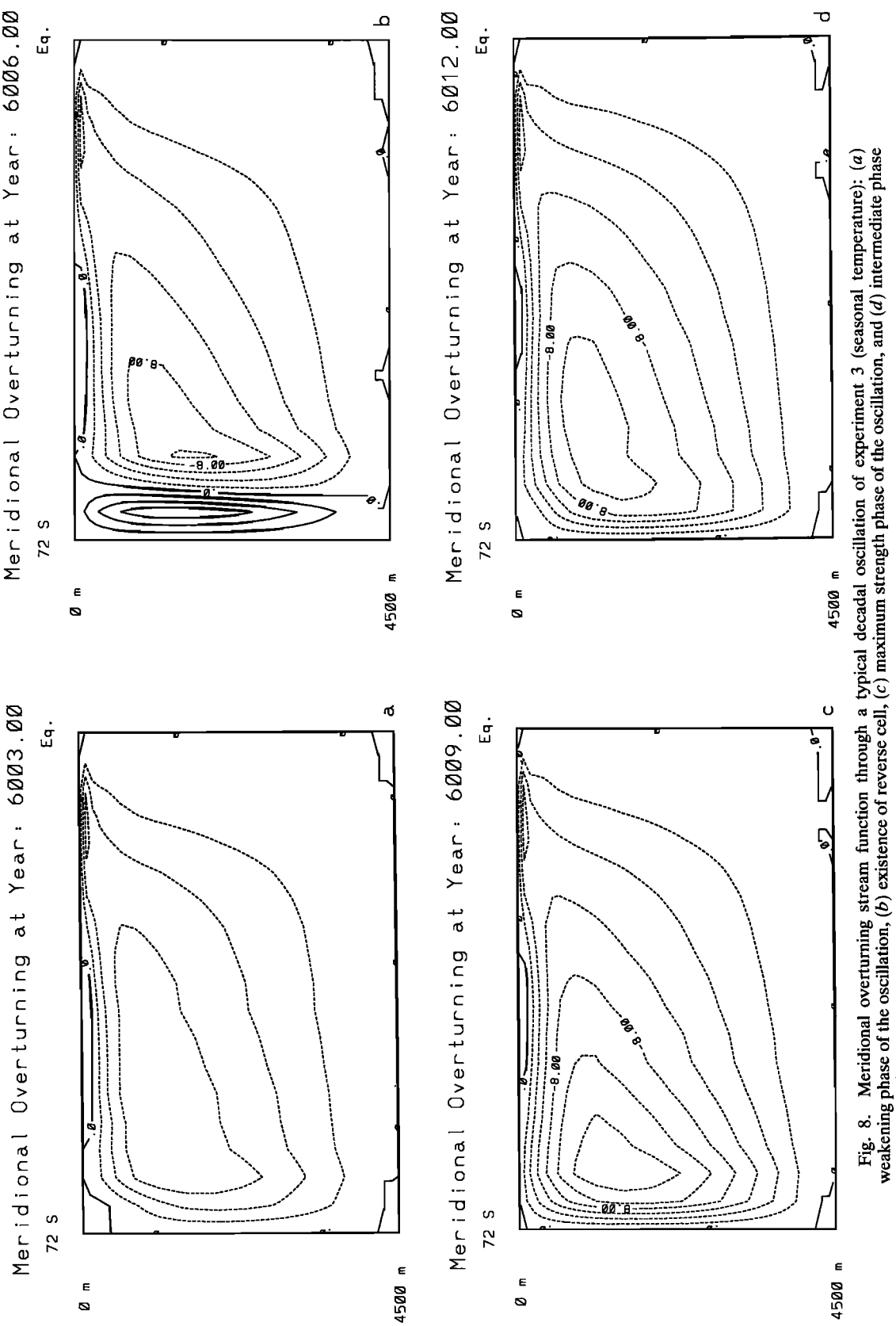

Fig. 8. Meridional overturning stream function through a typical decadal oscillation of experiment 3 (seasonal temperature): (*a*) weakening phase of the oscillation, (*b*) existence of reverse cell, (*c*) maximum strength phase of the oscillation, and (*d*) intermediate phase of the oscillation.

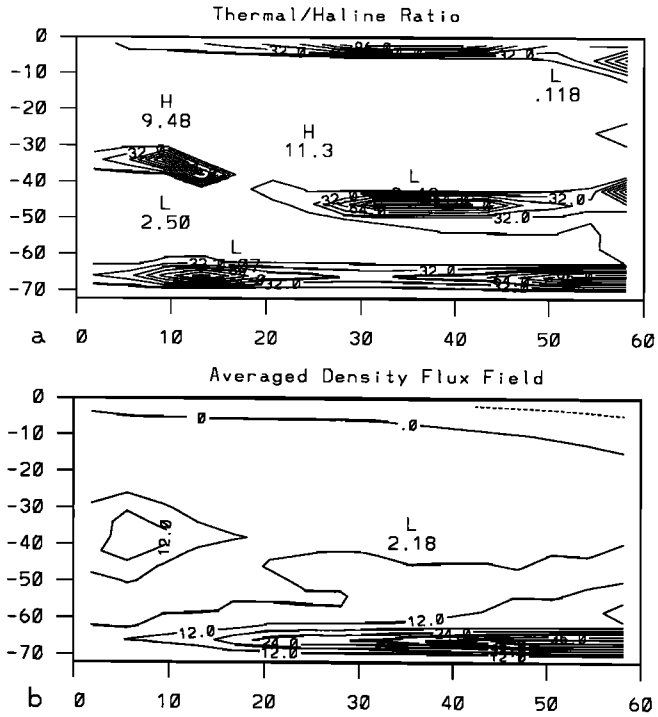

Fig. 9. (*a*) The absolute value of the ratio of the thermal to the haline effects on the density flux from experiment 3 (seasonal temperature) as obtained by annually averaging and averaging over a decadal oscillation (contour interval, 16.0). (*b*) Density flux field (10^{-6} kg/m^2 s) into the basin as obtained by annual averaging and averaging over an oscillation (contour interval, 6.0×10^{-6} kg/m^2 s).

3.9. *Experiment 8 (Reduced Seasonal Temperature)*

In this, our "reduced seasonal temperature" experiment, we lower the summer temperature at the polar boundary to 4.0°C. Otherwise, this experiment is the same as experiment 3 (seasonal temperature). The results resembled those of experiment 7 (amplified seasonal temperature), with a collapse, a period of irregular oscillations, followed by a series of flushes and collapses (Figure 14*a*). Small-scale oscillations are also present, although at a higher frequency than those found in the previous experiment (Figure 14*b*). The magnitude of the flushes was the smallest of any experiment (Figure 14*c*).

3.10. *Experiment 9 (Seasonal Winds)*

In this, the "seasonal winds" experiment, the surface wind stress forcing is allowed to vary over the course of a year. The basic wind regimes of easterlies at low latitudes, westerlies at mid-latitudes and polar easterlies is modified based on the data of *Hellerman and Rosenstein* [1983]. To represent the north-south movement of the subtropical high and the subpolar low over the course of the year, the lines dividing the different wind regimes (easterlies and westerlies) are allowed to move over the course of a year. This is simulated with a simple sine function

$$\Phi_z(t) = \left(3.0 \sin\left(t \frac{\pi}{365.0}\right) + \phi_{\text{lat}}\right) \frac{\pi}{180.0}$$

where Φ_z is the dividing latitude between the different wind regimes (in radians), ϕ_{lat} is the base latitude of the dividing line between the different wind regimes (and is 25.0° and 62.0°), and t is the day of the year.

The winds of each regime are then modified based on the fact that the subtropical high intensifies in summer and weakens in winter, while the subpolar low intensifies in winter and weakens in summer. The intrannual changes of the subpolar low are greater in magnitude than those of the subtropical high [*Moran and Morgan*, 1991]. In the region of low-latitude easterlies, the wind stress is modified such that

$$T^{\lambda}_{\text{least}}(\phi) = T^{\lambda}(\phi) + T^{\lambda}(\phi) \frac{1}{2} \left|\cos\left(t \frac{\pi}{365.0} + \frac{\pi}{2}\right)\right|$$

where $T^{\lambda}(\phi)$ is the basic annually averaged surface wind stress calculated in section 2. The westerlies of mid-latitudes are modified such that

$$T^{\lambda}_{m\text{west}}(\phi) = T^{\lambda}(\phi) + T^{\lambda}(\phi) \frac{1}{2} \left|\cos t \frac{\pi}{365.0}\right|$$

while the high latitude easterlies become

$$T^{\lambda}_{h\text{east}}(\phi) = T^{\lambda}(\phi) + T^{\lambda}(\phi) \frac{1}{2} \left|\cos\left(t \frac{\pi}{365.0} + \pi\right)\right|$$

These wind stresses are illustrated in Figure 15 for each season. In all other respects this experiment is the same as experiment 4 (synchronous seasonal temperature); i.e., integration is conducted synchronously.

The use of the seasonal wind field produces the depth-integrated transport seen in Figure 16*a* for summer and Figure 16*b* for winter. The flow is characterized by two strong gyres and a weaker equatorial gyre. The cyclonic subpolar gyre is intensified in winter, while the anticyclonic subtropical gyre is increased in strength in the summer.

This experiment was started from the end of the spin-up and was then integrated using fully synchronous integration for the reasons discussed in section 3.5. Upon the change from restoring to mixed boundary conditions, the circulation collapsed. Following this, the circulation increased in strength and began to oscillate irregularly. After about 700 years, the circulation settled down to a long period of fairly regular oscillations (Figure 17*a*). The power spectral density, which is almost exactly the same as that of experiment 4 (Figure 10*a*), reveals a strong decadal peak, with a period of around 11 years.

This experiment is limited by the coarse resolution of the model and the lack of topography, since it is known that seasonal wind-forced circulation has strong interactions with topography [*Greatbatch and Goulding*, 1989*a*, *b*]. However, it is not the purpose of this paper to investigate the effects of topography. For the purpose of this paper, the presence of decadal variability in this experiment shows that the variability is robust and that the use of annually averaged winds in the previous experiments is not a limitation.

This result is expected on the basis of a scale analysis that shows that the thermohaline effects are more important than the wind effects. Using the derivations of *Bryan* [1987], the "thermally driven" velocity scale u_t is

$$u_t = \left[\left(\frac{g\Delta\rho^*}{2\Omega\rho_0}\right)^2 A_{TV}/a\right]^{1/3}$$

where a is the radius of the Earth and is taken to be 6373 km, the acceleration due to gravity is taken to be 9.8 m/s^2, and ρ_0 is taken to be 1026 kg/m^3. $\Delta\rho^*/\rho_0$ is calculated based on the formula of *Bryan* [1987], with $\Delta\rho^*$ being the actual range of

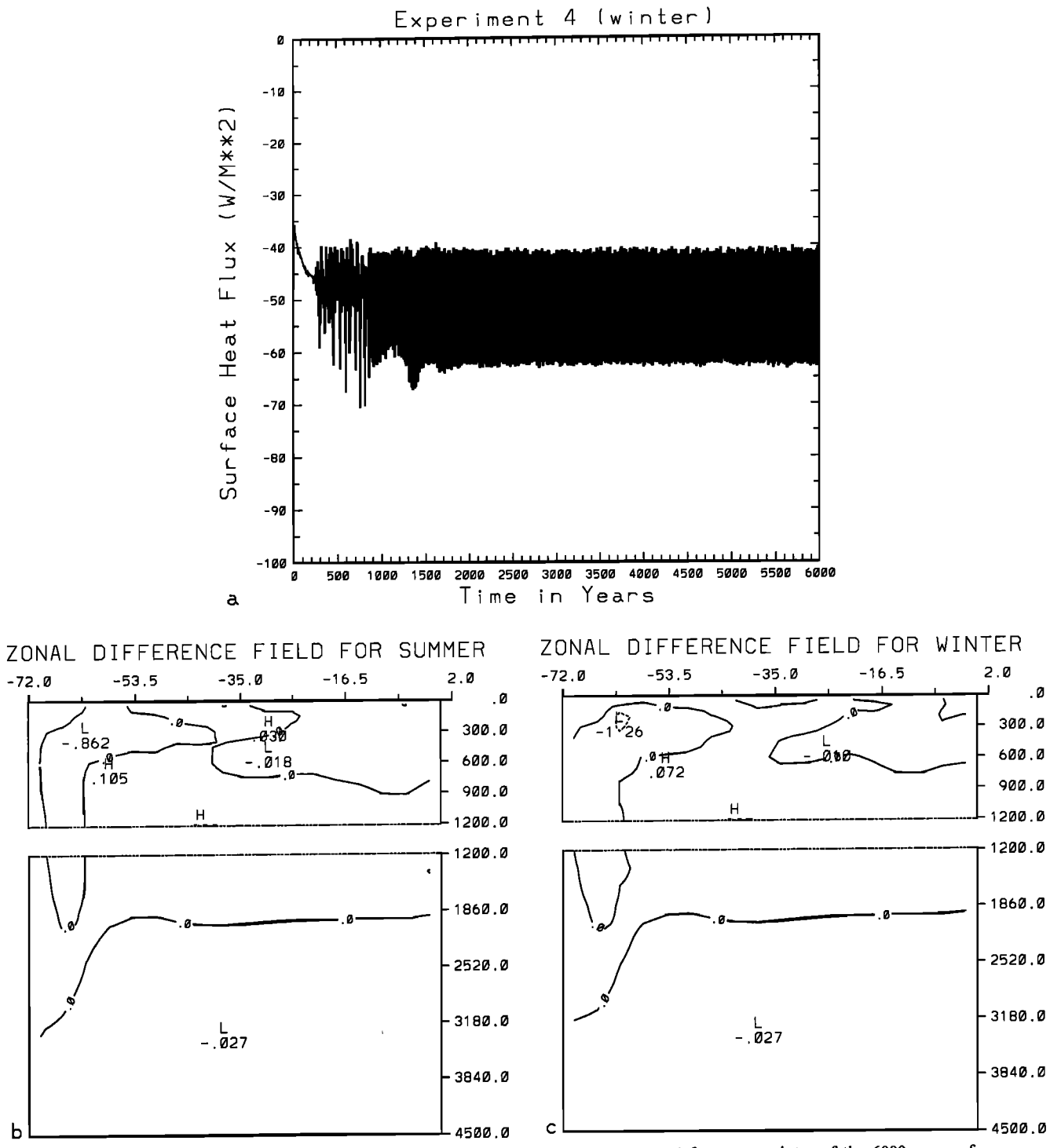

Fig. 10. (*a*) Net basin-averaged surface heat flux (watts per square meter) for every winter of the 6000 years of integration of experiment 4 (synchronous seasonal temperature), and difference field of zonal temperatures between experiments 3 (seasonal temperature) and 4 for (*b*) the summer and (*c*) the winter.

surface densities. The horizontal velocity scaling corresponding to the Sverdrup balance is

$$u_s = \frac{T^*}{\rho_0 2\Omega D}$$

where D is the depth of the basin and T^* is a measure of the range of magnitude of the zonal windstress. The ratio of these quantities $\gamma = u_s/u_t$ is a good measure of the relative strengths of the wind and thermal forcing.Calculating these quantities gives u_s = 0.9 cm/s and u_t = 1.37 cm/s, which gives γ = 0.72, giving the expected result that the thermal forcing is more important.

3.11. *Experiment 10 (No Winds)*

In our final experiment, experiment 10 ("No Winds"), we repeated experiment 3 but removed the surface wind forcing.

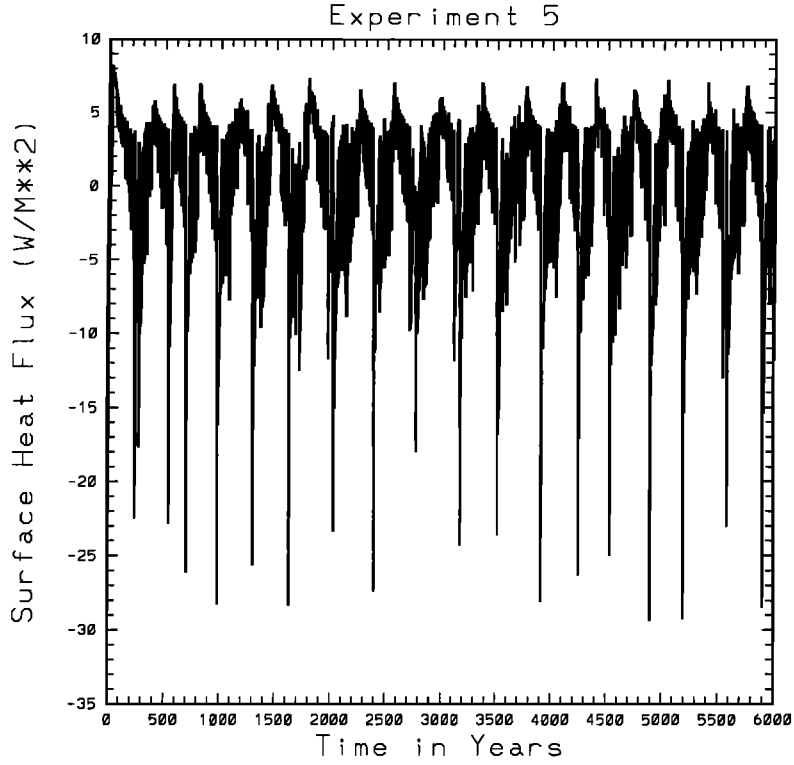

Fig. 11*a*. As in Figure 7*b* but for experiment 5 (seasonal freshwater flux).

With no surface wind forcing, the circulation quickly collapsed with the development of a polar halocline. The lack of wind-driven salt transport prevented the circulation from reestablishing itself [*Marotzke*, 1990]. Decadal variability existed in this collapsed state, interposed between strong flushes on the diffusive time scale (Figure 17*b*).

3.12. *Summary of Experiments*

In this section we showed that decadal/interdecadal variability of the thermohaline circulation may exist internally even in the presence of seasonal forcing. These time scales of variability are summarized in Table 3. The use of the acceleration techniques of *Bryan* [1984] was shown to have no important effect on the results, provided annually averaged wind forcing was used. We were able to produce different regimes of the thermohaline circulation by varying the maximum temperature of the seasonal cycle, these regimes being a sequence of collapses and flushes, and a circulation showing pronounced decadal variability. Flushes were found to be weaker and more frequent than those found in experiments without a seasonal cycle.

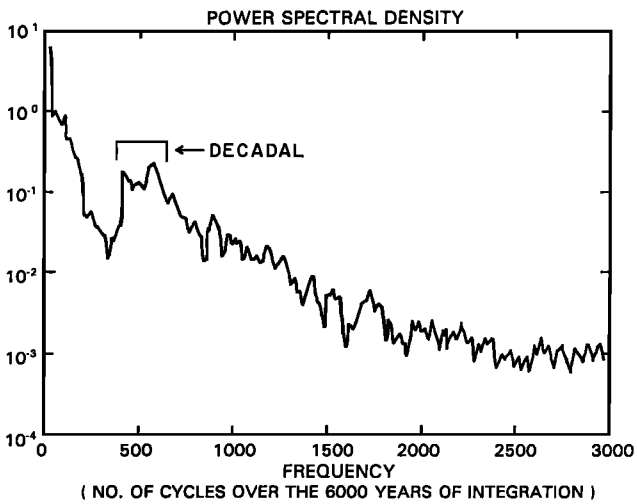

Fig. 11*b*. As in Figure 7*d* but for Figure 11*a* (experiment 5).

Another effect of the inclusion of the seasonal cycle was the effect it had on bottom water temperatures (Table 3). Since most deep water is formed at the surface in high latitudes, the deep ocean is very sensitive to polar amplification of temperature [*Manabe and Bryan*, 1985]. As one can see from the table, the bottom water temperatures increased quite markedly from experiment 1, which was without a seasonal cycle, to experiments 2–4, which had a seasonal cycle present. The lower bottom temperatures in experiment 2 (fully seasonal) are related to the lack of pronounced decadal variability in that experiment, when compared to experiments 3 (seasonal temperature) and 4 (synchronous seasonal temperature). In the latter two experiments, the strong oscillations in the stream function cause the site of deep water formation to be moved equatorward during part of the oscillation. As the surface waters are warmer at these lower latitudes where convection is now occurring, warmer water will be convected down to the deep ocean, producing warmer bottom water temperatures in experiments 3 and 4. Since the rest of our experiments never reached a seasonal equilibrium, we do not discuss their bottom water temperatures.

4. POLEWARD HEAT TRANSPORT

It has been noted that a very large fraction of the oceanic heat transport can be accounted for by the thermohaline circulation [*Bryan*, 1962], although this does not take into consideration an important contribution from the wind

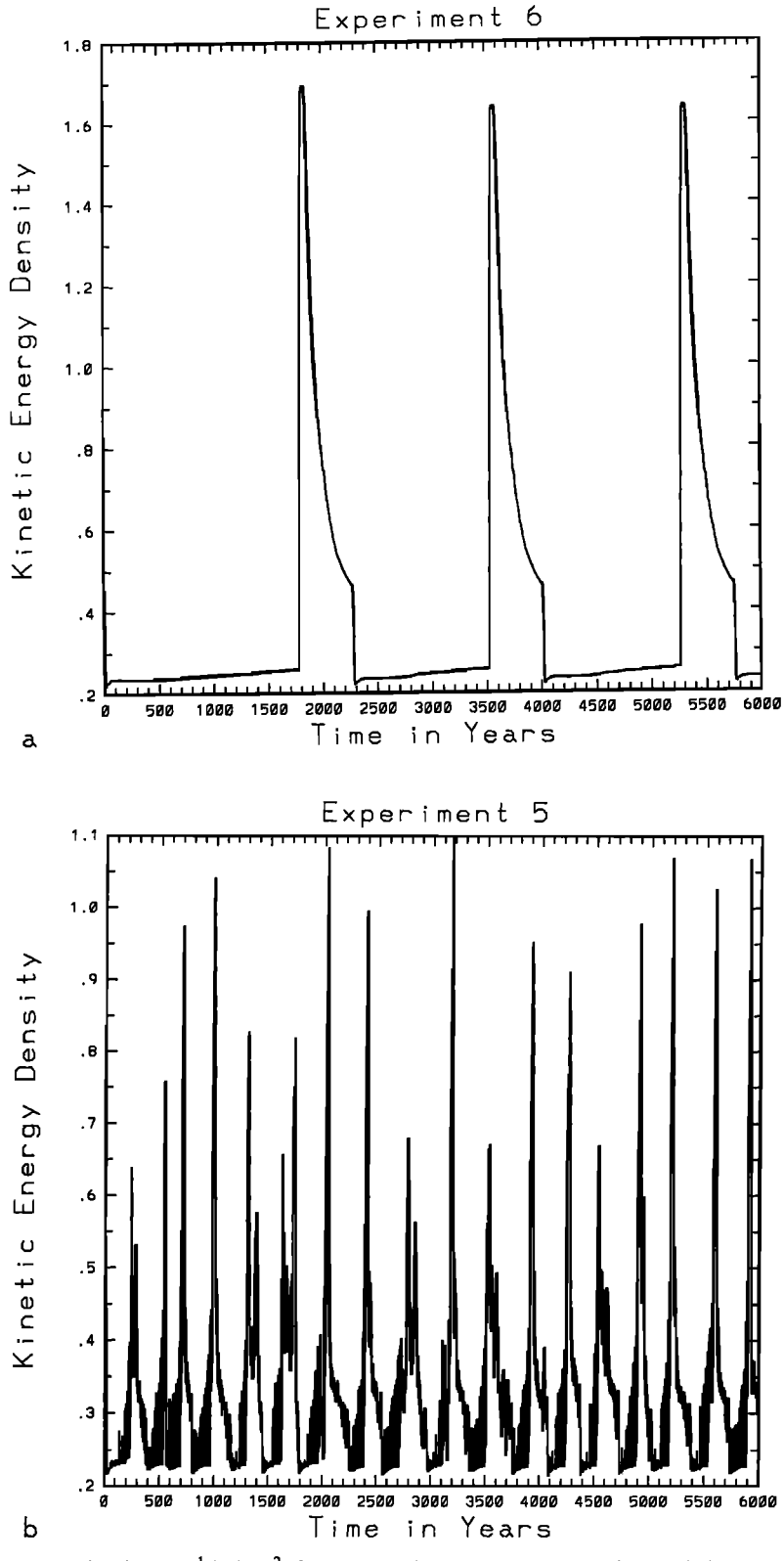

Fig. 12. Kinetic energy density (10^{-1} kg/m s^2) for (*a*) experiment 6 (perpetual spring) and (*b*) experiment 5 (seasonal freshwater flux).

[*Bryan et al.*, 1975]. Variations in the thermohaline circulation can therefore have substantial effect on the poleward heat transport. In this section we will show that such oscillations in the poleward heat transport exist in our seasonal model. It must be noted that the poleward heat transport in our model is much smaller than that estimated from observations [*Hall and Bryden*, 1982] owing to our basin symmetry condition which constrains the transport to be zero at the equator.

Our basic poleward heat transport profile, which is for experiment 2 (fully seasonal), is shown in Figure 18*a*. It reveals slight seasonal variations in the poleward heat trans-

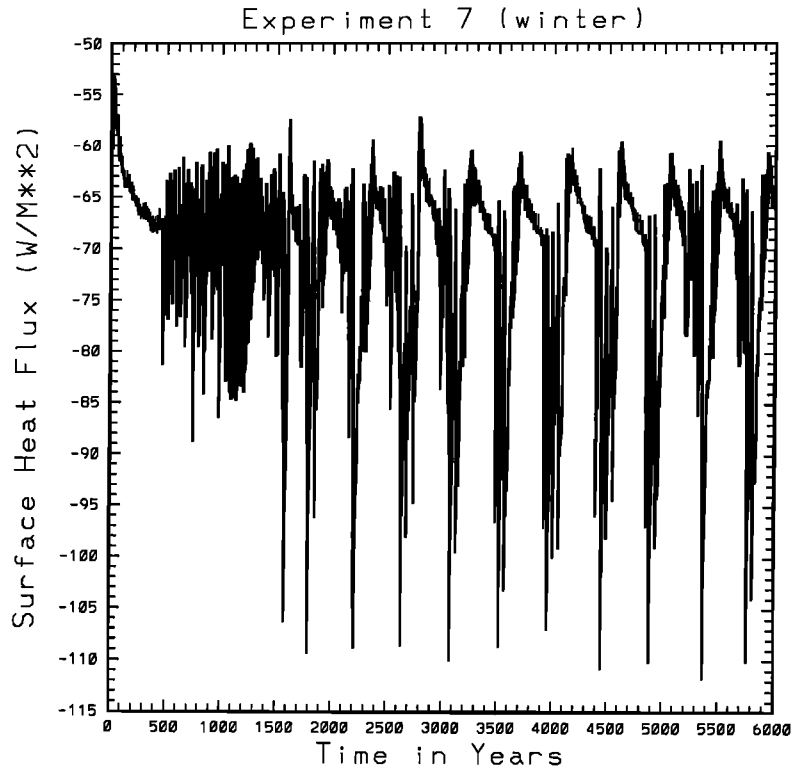

Fig. 13*a*. As in Figure 7*b* but for experiment 7 (amplified seasonal temperature).

port but no interannual variations, with the transport curves for each year falling directly overtop the preceding one. The lack of interannual changes are due to the fact that the thermohaline circulation is seasonally steady in this experiment. The same transport is shown for experiment 1 (perpetual winter) in Figure 18*b*. Again a steady thermohaline circulation means no interannual variations in the heat transport, while the lack of seasonal variations in the restoring temperature removes the intra-annual variations. The magnitude of the transport is stronger in the perpetual winter experiment, as there is a stronger meridional temperature gradient in that experiment than in the fully seasonal experiment.

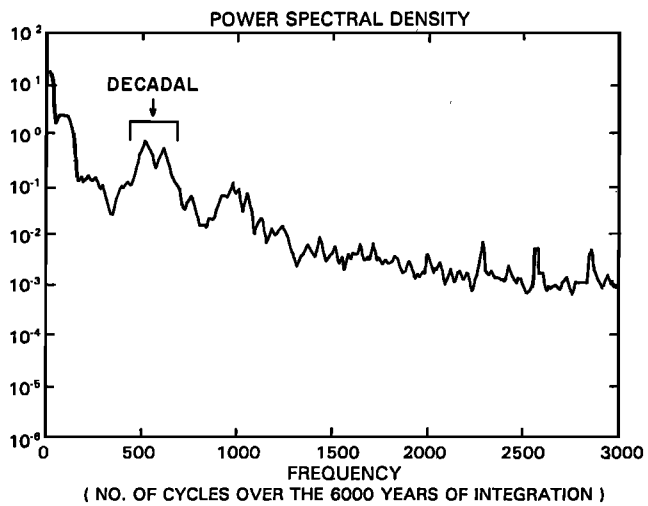

Fig. 13*b*. As in Figure 7*d* but for Figure 13*a* (experiment 7).

In the experiments where significant oscillations in the thermohaline circulation occur (experiments 3 and 5), these oscillations showed up in the poleward heat transport. Figures 18*c* and 18*d* show the transport in both the summer and winter, respectively, over a complete oscillation for experiment 3 (seasonal temperature). Large variations occur over the period of the oscillation, with the maximum transport corresponding to the time when deep water is being formed at the polar boundaries and the circulation is the most vigorous. The variability in the strength of the poleward heat transport is greater over the course of the decadal oscillation than the change in the transport through the annual cycle. The absolute magnitude of the transport is weaker in the seasonal temperature experiment than in the previous two because the overall circulation is weaker, and therefore less heat is transported poleward. Similar variations were observed in experiment 5 (seasonal freshwater flux) (Figure 18*e*), except that the variability in the transport is larger by a factor of at least 2. This can be attributed to the sensitivity of convection, and therefore thermohaline circulation to even minor changes in the freshwater flux and the freshwater flux varies greatly over the course of a year in this experiment.

5. Discussion and Summary

In this paper we have found that decadal variability exists under seasonal forcing. That is, despite forcing the system with a strong subannual signal, the system may respond with energy at the decadal or longer time scale. This result is significant, as it shows that decadal variability is robust under time dependent forcing and is not an artifact of the steady surface boundary conditions used in previous models [*Weaver and Sarachik*, 1991*a*, *b*].

The existence of decadal/interdecadal variability in this

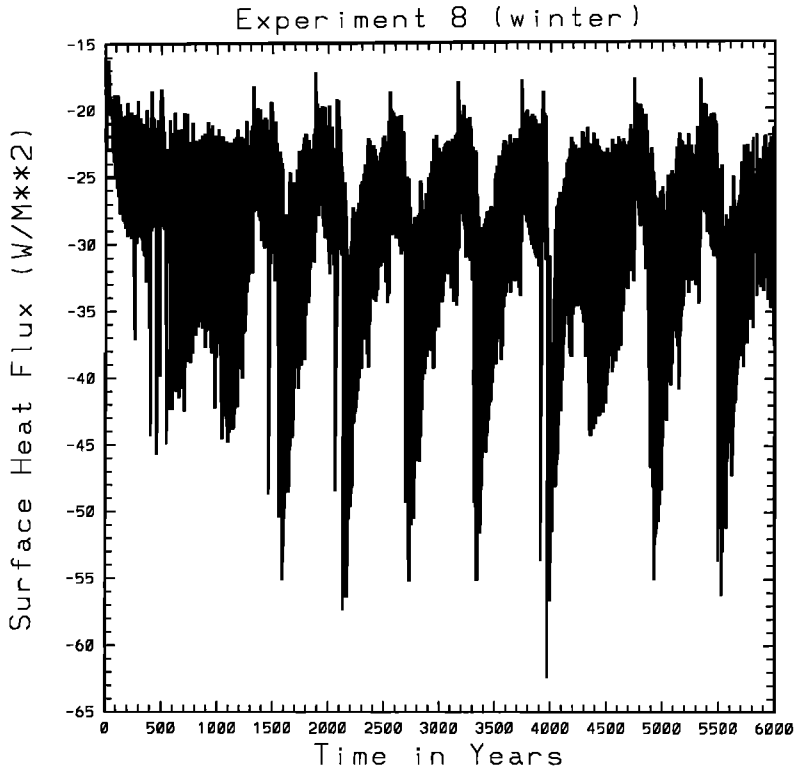

Fig. 14*a*. As in Figure 7*b* but for experiment 8 (reduced seasonal temperature).

simulation is linked to the existence of a local maximum in the net density flux forcing field associated with a local *P-E* minimum. Warm, saline water is produced around 45°S by a *Welander* [1982] type oscillator. This water is then advected eastward and then poleward into the region of strong density gain, which causes deep convection to occur. This region of positive density flux, and hence convection, increases in size zonally as more warm, saline water is advected into this area, causing the zonal pressure gradient to be weakened. This decreases the strength of the meridional overturning.

Eventually, when the high-latitude region is cut off from its source, the anomaly in the convective region, around 65°S, begins to shrink. This causes the region of strong density gain to decrease in size, increasing the zonal pressure gradient and thereby causing the thermohaline circulation to intensify. The oscillation then begins anew.

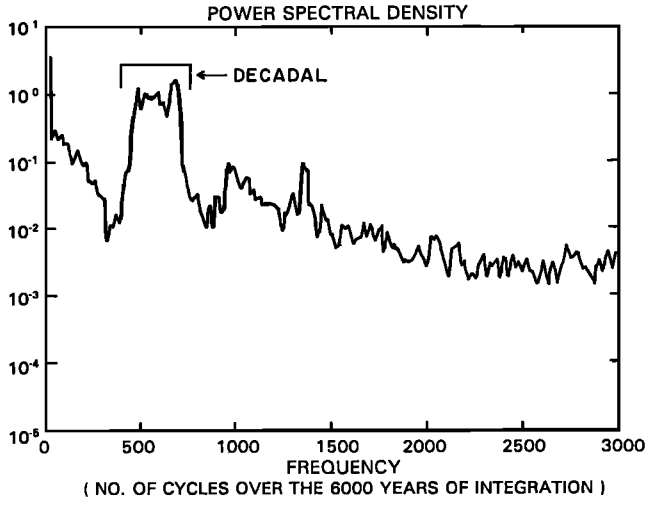

Fig. 14*b*. As in Figure 7*d* but for Figure 14*a* (experiment 8).

The variability exists in our seasonal temperature experiment (experiment 3) despite having high-latitude freshening year round (Figure 4). This implies that the oscillation is a combined temperature and salinity effect, which agrees with the results of *Schmitt et al.* [1989], who showed that although salt may dominate the density field at the ice-water interface, fresh water does not dominate the density fluxes in the high-latitude open ocean.

Decadal/interdecadal variability exists under both annual mean and seasonal *P-E* forcing. Since the *P-E* forcing field has large seasonal variance [*Schmitt et al.*, 1989], this robustness is a welcome result. Since the decadal variability is mainly an internal thermal and haline process, annually varying winds were also shown to have no significant effect on the internal variability.

The presence of the seasonal cycle on the freshwater flux constrains the time of year when deep convection can occur. By increasing the magnitude of the freshening that occurs in winter, the seasonally varying freshwater flux field is able to curtail convection and cause the circulation to collapse.

Flushes were shown to exist under seasonal forcing. The inclusion of seasonal forcing increases the frequency of the flushes by reducing the critical temperature at which static instability occurs. As well, the flushes under seasonal forcing are weaker, producing variability in the basin-averaged net surface heat flux of the order of 20–50 W/m^2 on the century time scale.

All our experiments were performed in one hemisphere, which would seem to exclude potentially significant interhemispheric exchanges. However, *Weaver and Sarachik*

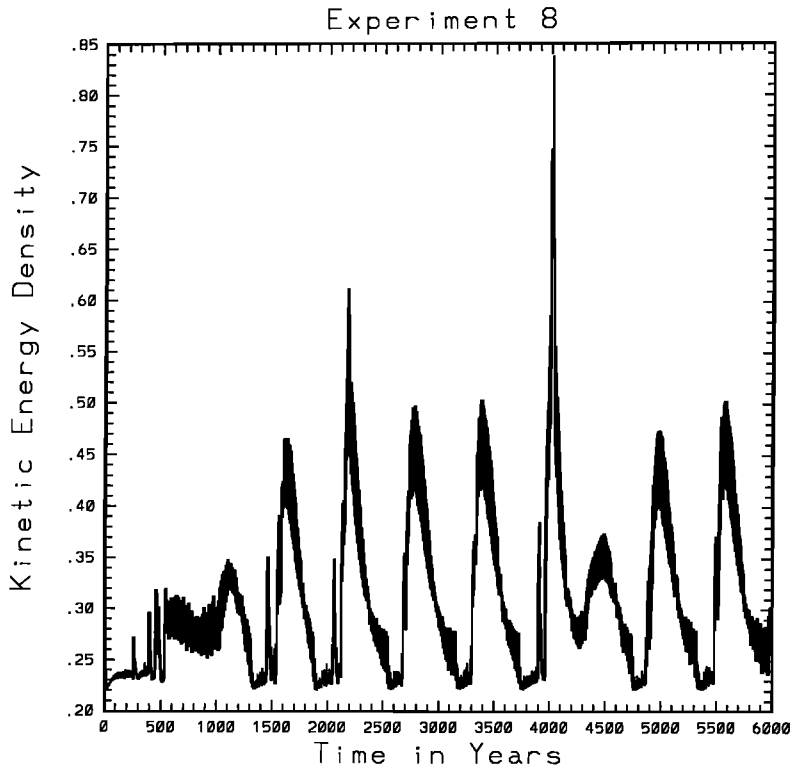

Fig. 14*c*. Kinetic energy density (10^{-1} kg/m s^2) for experiment 8.

[1991*a*] showed in a series of two-hemisphere experiments that the decadal variability was a single hemisphere phenomenon which appeared to act almost independently of the dynamics of the other hemisphere. They showed that changing from one hemisphere to two did change the structure of the flushes (i.e., they were of one-cell, pole-to-pole structure), but the underlying physics was the same as in one-hemisphere experiments.

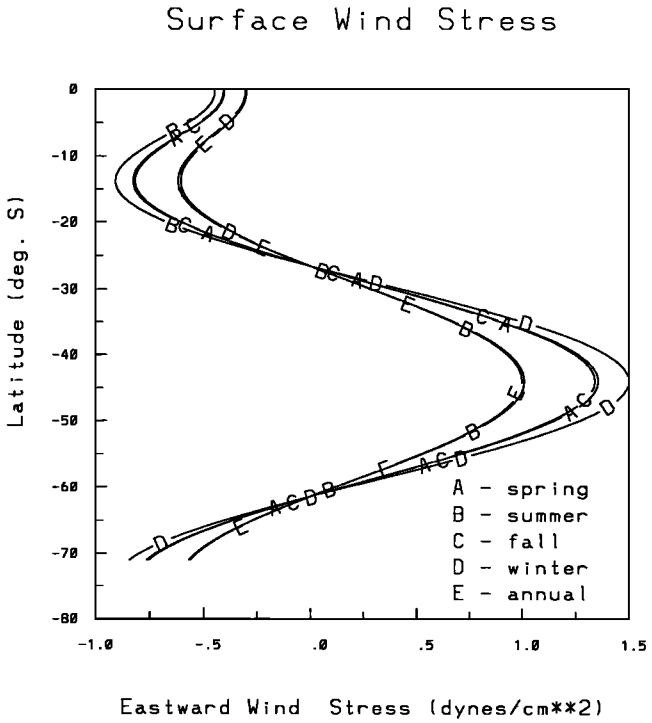

Fig. 15. Surface seasonal zonal wind stress (dynes per square centimeter) used to force experiment 9 (seasonal winds) and the annual mean surface zonal wind stress.

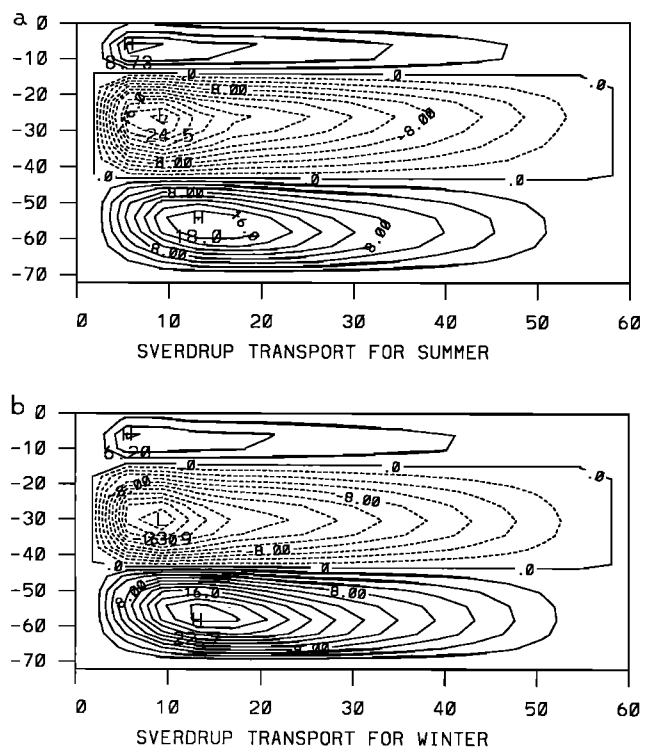

Fig. 16. Wind-driven transport for experiment 9 for (*a*) summer and (*b*) winter.

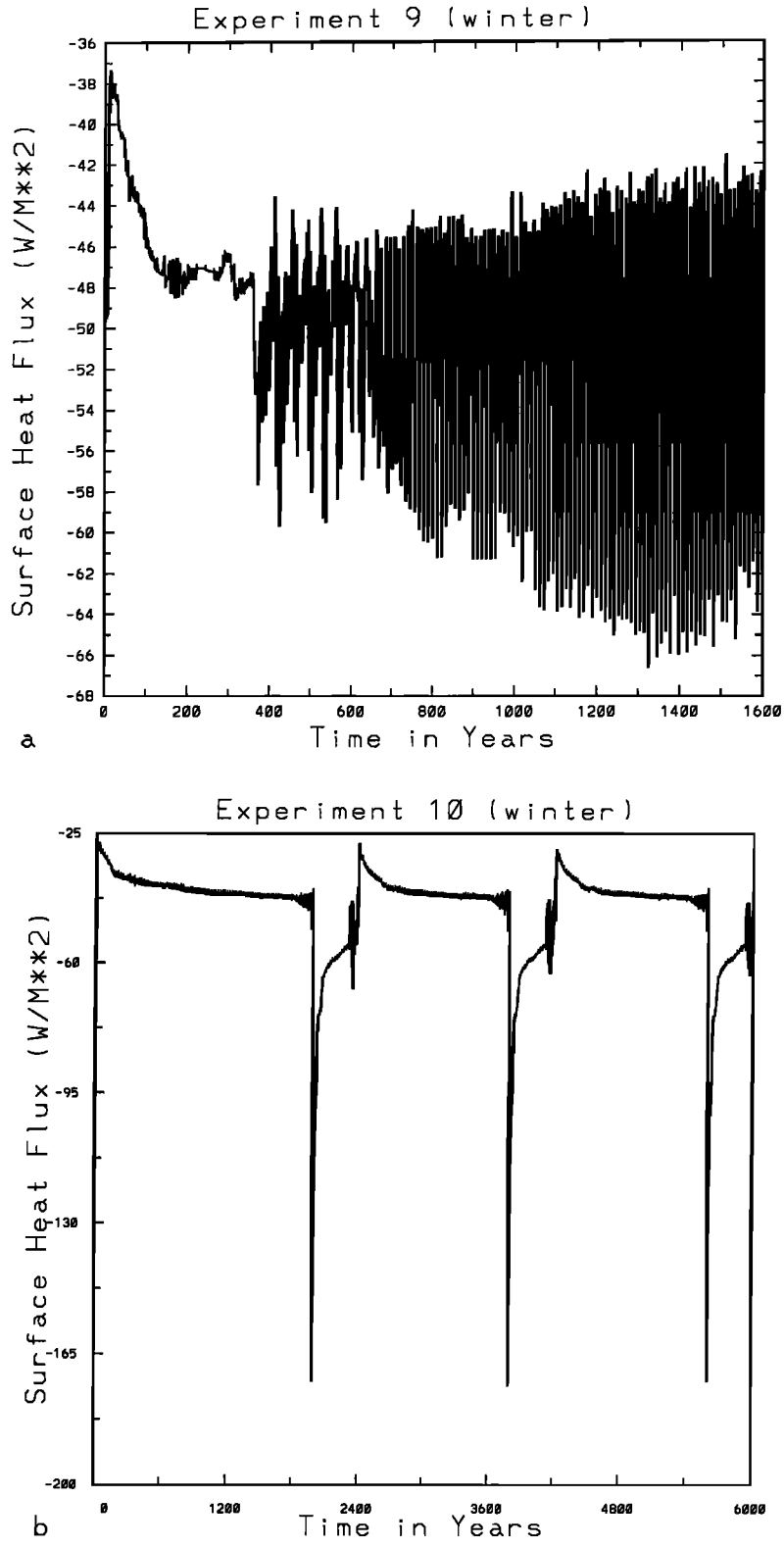

Fig. 17. Net basin-averaged surface heat flux (watts per square meter) for (*a*) every winter of 1600 years of synchronous integration of experiment 9 (seasonal winds) and (*b*) every winter of the 6000 years of integration of experiment 10 (no winds).

Our experiments with a seasonal cycle on temperature show the sensitivity of the thermohaline circulation to the magnitude of the summer warming. Depending on whether the summer amplitude fell within a given range or not, we were able to produce different regimes of the thermohaline circulation. If the summer polar restoring temperature is within this range, a steady circulation with decadal variability developed. Otherwise, it collapsed, leading to a sequence

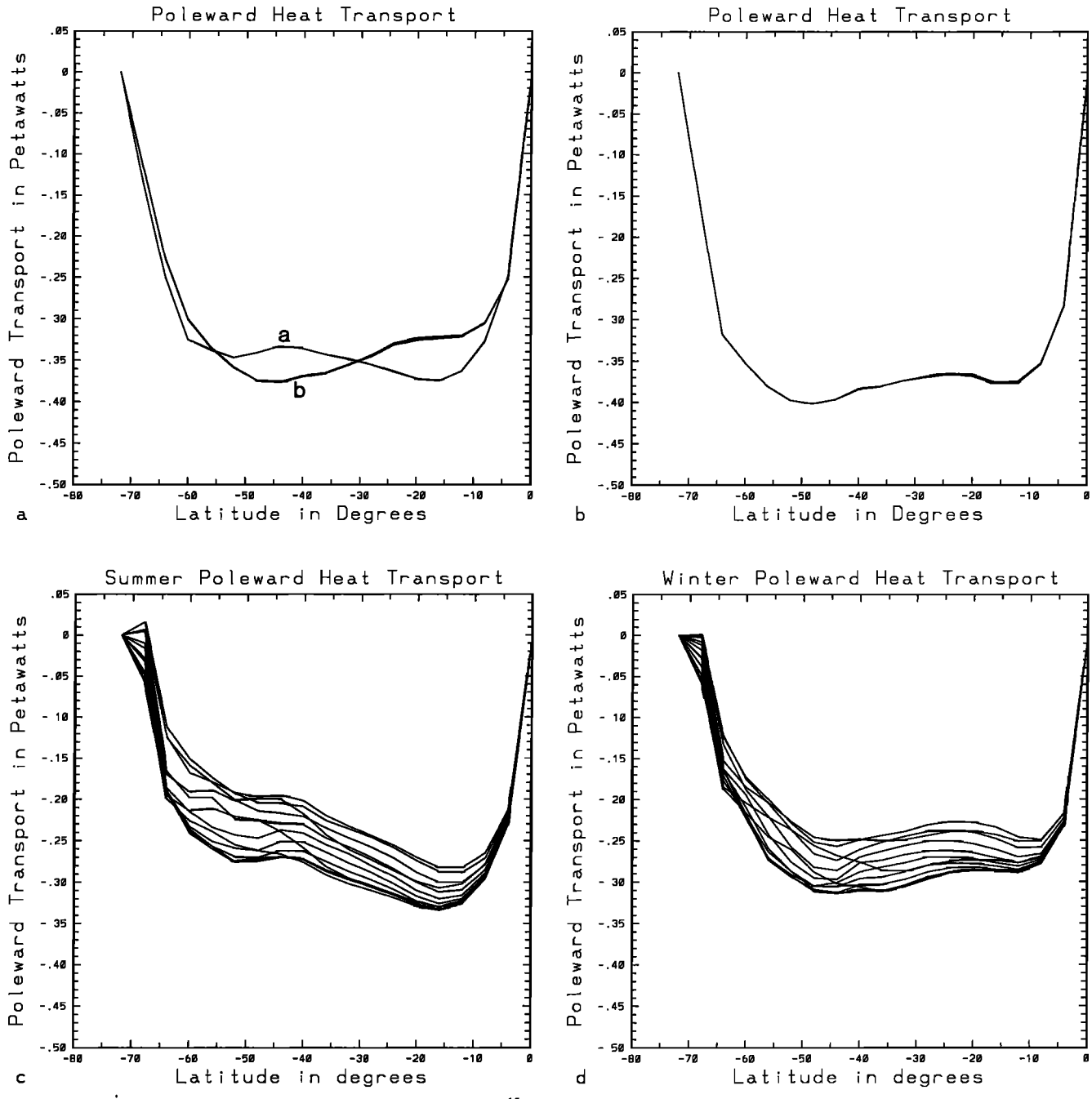

Fig. 18. Poleward heat transport in petawatts (10^{15} W) for (*a*) experiment 2 (summer, line a; winter, line b), (*b*) experiment 1 (summer and winter), (*c*) experiment 3 (summer), (*d*) experiment 3 (winter), and (*e*) experiment 5 (summer and winter). Note that Figure 18*e* only shows the variability in the poleward heat transport over the decadal oscillation and not during a flush.

of flushes and collapses, with some decadal variability superimposed.

Another important point to mention is that even when a seasonal cycle is present under restoring boundary conditions, the meridional overturning does not change much over the course of the year. Although convection is suppressed in the summer, thereby reducing zonal pressure gradients in the upper levels at high latitudes, the inertia of the thermohaline circulation is such that it remains largely unaffected by the relatively high frequency seasonal surface forcing. This is why changes in the poleward heat transport are greater over the course of the decadal oscillation, even in summer, than those changes through the year.

In summary, the most important conclusion of this paper is that internal variability of the thermohaline circulation, on decadal and longer time scales, can exist even under strong seasonal forcing. Accuracy in determining the magnitudes of the seasonal cycle on temperature and freshwater flux is important as the circulation is sensitive to changes in both. The seasonal cycle also acts to curb the magnitudes of flushes and produces frequencies that may have relevance in the interpretation of long-term climate records.

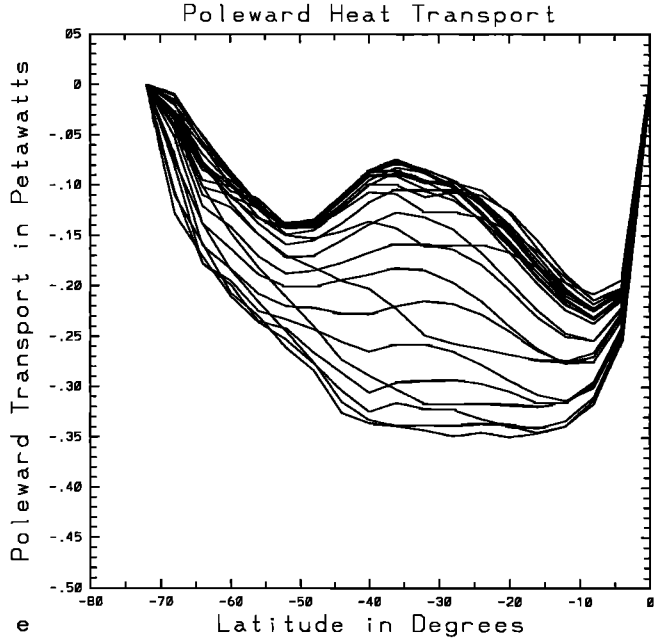

Fig. 18. (continued)

Acknowledgments. This study forms the basis of P.M.'s M.Sc. thesis, completed in the Department of Meteorology, McGill University, and was supported through NSERC, AES, and FCAR operating grants awarded to A.J.W. We would like to thank Tertia Hughes for carefully reading an earlier version of this manuscript and providing detailed comments. P.M. would also like to thank William Gough and Richard Greatbatch for their helpful comments.

REFERENCES

Bryan, F., Maintenance and variability of the thermohaline circulation, Ph.D. thesis, Princeton Univ., Princeton, N. J., 1986.

Bryan, F., Parameter sensitivity of primitive equation ocean general circulation models, *J. Phys. Oceanogr.*, *17*, 970–985, 1987.

Bryan, K., Measurements of meridional heat transport by ocean currents, *J. Geophys. Res.*, *67*, 3403–3414, 1962.

Bryan, K., Accelerating the convergence to equilibrium of ocean-climate models, *J. Phys. Oceanogr.*, *14*, 666–673, 1984.

Bryan, K., and M. D. Cox, An approximate equation of state for numerical models of ocean circulation, *J. Phys. Oceanogr.*, *2*, 510–514, 1972.

Bryan, K., S. Manabe, and R. C. Pacanowski, A global ocean-atmosphere climate model, II, The oceanic circulation, *J. Phys. Oceanogr.*, *5*, 30–46, 1975.

Cattle, H., Diverting Soviet rivers: Some possible repercussions for the Arctic Ocean, *Polar Rec.*, *22*, 485–498, 1985.

Cox, M. D., A primitive equation, three-dimensional model of the ocean, *GFDL Ocean Group Tech. Rep. 1*, NOAA Geophys. Fluid Dyn. Lab., Princeton Univ., Princeton, N. J., 1984.

Crowley, T. J., Paleoclimate modelling, in *Physically-Based Modelling of Climate and Climate Change—Part II*, edited by M. E. Schlesinger, pp. 883–949, Kluwer Academic, Boston, Mass., 1988.

Dickson, R. R., J. Meincke, S.-A. Malmberg, and A. J. Lee, The "Great Salinity Anomaly" in the northern North Atlantic 1968–1982, *Prog. Oceanogr.*, *20*, 103–151, 1988.

Ghil, M., and R. Vautard, Interdecadal oscillations and the warming trend in global temperature time series, *Nature*, *350*, 324–327, 1991.

Gill, A. E., *Atmosphere-Ocean Dynamics*, Academic, San Diego, Calif., 1982.

Gray, W. M., Strong association between west African rainfall and U.S. landfall of intense hurricanes, *Science*, *249*, 1251–1256, 1990.

Greatbatch, R. J., and A. Goulding, Seasonal variations in a linear barotropic model of the North Atlantic driven by the Hellerman and Rosenstein wind stress field, *J. Phys. Oceanogr.*, *19*, 572–595, 1989*a*.

Greatbatch, R. J., and A. Goulding, Seasonal variations in a linear barotropic model of the North Pacific driven by the Hellerman and Rosenstein wind stress field, *J. Geophys. Res.*, *94*, 12,645–12,665, 1989*b*.

Hall, M. M., and H. L. Bryden, Direct estimates and mechanisms of ocean heat transport, *Deep Sea Res.*, *29*, 339–359, 1982.

Haney, R. L., Surface thermal boundary condition for ocean circulation models, *J. Phys. Oceanogr.*, *1*, 241–248, 1971.

Hasselmann, K., An ocean model for climate variability studies, *Prog. Oceanogr.*, *11*, 69–92, 1982.

Hellerman, S., and M. Rosenstein, Normal monthly wind stress over the world ocean with error estimates, *J. Phys. Oceanogr.*, *13*, 1093–1104, 1983.

Hibler, W. D., III, and S. J. Johnsen, The 20-year cycle in Greenland ice core records, *Nature*, *280*, 481–483, 1979.

Ikeda, M., Decadal oscillations of the air-ice-ocean system in the northern hemisphere, *Atmos. Ocean*, *28*, 106–139, 1990.

Krishnamurti, T. N., S.-H. Chu, and W. Iglesias, On the sea level pressure of the Southern Oscillation, *Arch. Meteorol. Geophys. Bioclimatol., Ser. A*, *34*, 385–425, 1986.

Lazier, J. R. N., Oceanographic conditions at O. W. S. Bravo 1964–1974, *Atmos. Ocean*, *18*, 227–238, 1980.

Levitus, S., Climatological atlas of the world ocean, *NOAA Prof. Pap. 13*, Natl. Oceanic and Atmos. Admin., Rockville, Md., 1992.

Manabe, S., and K. Bryan, CO_2-induced change in a coupled ocean-atmosphere model and its paleoclimatic implications, *J. Geophys. Res.*, *90*, 11,689–11,707, 1985.

Marotzke, J., Instabilities and multiple equilibria of the thermohaline circulation, Ph.D. thesis, *Ber. 194*, 126 pp., Inst. für Meereskd., Univ. Kiel, Kiel, Germany, 1990.

Moran, J. M., and M. D. Morgan, *Meteorology: The Atmosphere and the Science of Weather*, Collier Macmillan, Toronto, 1991.

Myers, P. G., Seasonal forcing and low-frequency variability of the thermohaline circulation, M.Sc. thesis, McGill Univ., Montreal, Quebec, Canada, 1992.

Mysak, L. A., and D. K. Manak, Arctic sea-ice extent and anomalies, 1953–1984, *Atmos. Ocean*, *27*, 376–405, 1989.

Mysak, L. A., D. K. Manak, and R. F. Marsden, Sea-ice anomalies observed in the Greenland and Labrador seas during 1901–1984 and their relation to an interdecadal Arctic climate cycle, *Clim. Dyn.*, *5*, 111–133, 1990.

Schlosser, P., G. Banisch, M. Rhien, and R. Bayer, Reduction of deepwater formation in the Greenland Sea during the 1980's: Evidence for tracer data, *Science*, *251*, 1054–1056, 1991.

Schmitt, R. W., P. S. Bogden, and C. E. Dorman, Evaporation minus precipitation and density fluxes for the North Atlantic, *J. Phys. Oceanogr.*, *19*, 1208–1221, 1989.

Washington, W., and G. Meehl, Climate sensitivity due to increased CO_2: Experiments with a coupled atmosphere and ocean general circulation model, *Clim. Dyna.*, *4*, 1–38, 1989.

Weaver, A. J., and E. S. Sarachik, The role of mixed boundary conditions in numerical models of the ocean's climate, *J. Phys. Oceanogr.*, *25*, 1470–1495, 1991*a*.

Weaver, A. J., and E. S. Sarachik, Evidence for decadal variability in an ocean general circulation model: An advective mechanism, *Atmos. Ocean*, *29*, 197–231, 1991*b*.

Weaver, A. J., E. S. Sarachik, and J. Marotzke, Freshwater flux forcing of decadal and interdecadal variability, *Nature*, *353*, 836–838, 1991.

Weaver, A. J., J. Marotzke, P. F. Cummins, and E. S. Sarachik, Stability and variability of the thermohaline circulation, *J. Phys. Oceanogr.*, in press, 1992.

Welander, P., A simple heat-salt oscillator, *Dyn. Atmos. Oceans*, *6*, 232–242, 1982.

Wetherald, R. T., and S. Manabe, Response of the joint ocean-atmosphere model to the seasonal variation of solar radiation, *Mon. Weather Rev.*, *100*, 42–59, 1972.

Wright, D. G., and T. F. Stocker, A zonally averaged ocean model for the thermohaline circulation, I, Model development and flow development, *J. Phys. Oceanogr.*, *21*, 1713–1724, 1991.

P. G. Myers and A. J. Weaver, School of Earth and Ocean Sciences, University of Victoria, P. O. Box 3055, Victoria, British Columbia, Canada V8W 3P6.

(Received December 2, 1991;
revised February 19, 1992;
accepted February 20, 1992.)